JET CROSS FLOW INTERACTION: DEVELOPMENT OF AN EXPERINEMTAL SET UP AND PARAMETRIC STUDIES

by
Shantanu Pramanik

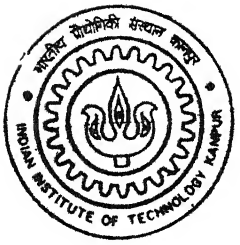

DEPARTMENT OF MECHANICAL ENGINEERING
INDIAN INSTITUTE OF TECHNOLOGY KANPUR
March, 2000

JET CROSS FLOW INTERACTION: DEVELOPMENT OF AN EXPERIMENTAL SET UP AND PARAMETRIC STUDIES

A Thesis Submitted
in Partial Fulfillment of the Requirements
for the Degree of
Master's of Technology

by
Shantanu Pramanik

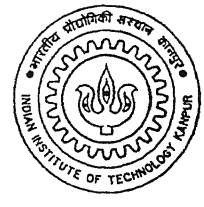

to the
Department of Mechanical Engineering
Indian Institute of Technology, Kanpur
March, 2000

to my parents

to my parents

Certificate

This is to certify that the thesis entitled **"JET-CROSS FLOW INTERACTION: DEVELOPMENT OF AN EXPERIMENTAL SET UP AND PARAMETRIC STUDIES"** by Mr Shantanu Pramanik has been carried out under my supervision The contents of this thesis have not been submitted and will not be submitted to any other Institute or University for the award of any degree and diploma

Subrata Sarkar

(Dr Subrata Sarkar)

Assistance Professor ,
Department of Mechanical Engineering,
Indian Institute of Technology Kanpur,
Kanpur-208016

19 th March, 2000

ACKNOWLEDGEMENT

It is my pleasure to express my sincere gratitude to Dr S Sarkar of Mechanical Engineering Department for his invaluable guidance and constant encouragement throughout the course of the present investigation I am also indebted to other faculty members of Mechanical Engineering Department for their valuable suggestions

I extend my thanks to the staff members of TA202 Laboratory for their constant support during the fabrication and installation of the test set-up I am also thankful to the staff members of Energy Conversion Laboratory for their assistance during the experimental work I am grateful to Mr S N Sharma, of Fluid Mechanics Laboratory for his help and support during the instrumentation of the test set-up

My thanks are also due to my friends Mr Sudipta De and Mr Sandip Dhar for their continuous support and inspiration during the experiment and compilation of the thesis report

I gratefully acknowledge the financial support from Mechanical Engineering Department without which it would not be possible to complete this work

CONTENTS

ABSTRACT

Film cooling of gas turbine blades is one of the practical examples of jet-crossflow interaction High performance gas turbine engines require cooling of turbine blades to protect them from thermal stresses created by the exposure of hot combustion gases In the blade cooling process, the compressor bleed air is introduced in the hollow core of each blade and then injected through rows of holes made along the pressure and suction surfaces of the blades The injected coolant is expected to form an insulating layer and thus, protects the blade surfaces from hot main stream Film cooling performance is affected by a number of flow and geometric parameters Geometric parameters that affect the film cooling include injection angle, pitch-to-diameter ratio, length-to-diameter ratio, hole exit shape and orientation with respect to the mainstream and also the blade curvature Flow parameters include the ratios of density, velocity and mass flux between the injectant and the mainstream, incoming boundary layer thickness and character, free-stream turbulence intensity and mainstream pressure gradient In our experimental set up, an instrumented test plate is placed on the inner bottom surface of the test section The test plate consists of three parts a leading edge plate, an insertable type plate with injection holes, and an adiabatic plate with temperature sensors placed at different strategic locations The hole-configurations considered here resemble the actual film cooling holes of turbine blades The tips of the temperature sensors have been flushed with the surface to avoid flow disturbances due to any protrusion within the flow domain All the outer surfaces of the test section were covered with low conductivity black foam to minimize the conduction of heat from the test section to the atmosphere

In a single experimental or computational study, it is difficult to study all the parameters that influence the film cooling performance For the present study, it was decided to experimentally investigate the effect of hole geometry on jet-crossflow interactions for different blowing and temperature ratios The aim of the work is to arrive at a hole-configuration, which can minimize the near-field non uniformity in the lateral variation of film effectiveness created by the injection of the discrete jets into the mainstream To achieve this, a low speed wind tunnel has been fabricated with provision of heating units both in the mainstream and the secondary flow circuit

However, the fabrication of primary heating unit, which can control the mainstream temperature has not yet been over The situation compelled us to use hot secondary air instead of colder one with respect to the mainstream The presence of hot injected fluid downstream of the holes was felt by measuring the surface temperature Although in stead of film cooling, it has modeled film heating, but the situation has not prevented us to define film effectiveness and thus, to examine the relative effect of geometry on the formation of film over the surface for different blowing and density ratios

The present investigation indicates that the moderate blowing ratio (B R.=1 0) produces better overall film effectiveness and increase of density ratio is always beneficial The near-field three-dimensionality in effectiveness is remarkably reduced by compound angle injection, which provides better protection of the regions between the holes, however, the downstream effectiveness is affected as a result of high rate of mixing between the two fluids

NOMENCLATURE

BR	blowing ratio
DR	density ratio
MR	momentum ratio
VR	velocity ratio
D	diameter of blowing hole
L	length of blowing hole
P	pitch
h_0	heat transfer coefficient without film cooling
h_f	heat transfer coefficient with film cooling
β	ratio of diameters for orifice meter
Q	volume flow rate of secondary air
p	pressure
A_t	throat area of *vena-contracta*
A_J	total area of injection
q''	wall heat flux
η_{ad}	adiabatic film effectiveness
T_∞	free-stream temperature
T_{aw}	adiabatic wall temperature
T_J	temperature of the jet at the hole exit
T_p	temperature of secondary air inside the plenum chamber
θ	ratio of temperature difference $= \left(\frac{T_\infty - T_J}{T_\infty - T_w}\right)$
C_d	discharge coefficient of orifice meter
δ^*	displacement thickness
δ^{**}	momentum thickness
H	boundary layer shape factor

c_p	specific heat of air at constant pressure
C_0	constant
$\tilde{L}$	characteristic length

Subscripts

J	jet condition
∞	free-stream condition
aw	adiabatic wall condition
w	wall condition
ad	adiabatic condition
f	condition with film cooling
0	condition without film cooling
t	throat condition
p	plenum chamber condition

LIST OF FIGURES

LIST OF TABLES

LIST OF CHARTS

CHAPTER 1

INTRODUCTION

1.1 Introduction

Modern aero engines are characterised by their high power output, low specific fuel consumption and low weight-to-power ratio One of the major contributing factors towards this achievement is the use of high turbine entry gas temperature Modern gas turbine engines are designed to operate at inlet temperatures of 1800-2000 K, which are beyond the highest allowable temperature for the conventional blade material used So, the blades need to be cooled to satisfy the safe operating conditions Discrete jet film cooling in conjunction with internal convective cooling is an effective way to achieve this objective

1.2 General Description of Film Cooling

Early investigations were mostly devoted the to two-dimensional film cooling created by the ejection of cold air through a continuous slot The flow field near the injected coolant jet is very complex even for slot injection with formation of a shear layer that separates the injected flow and the freestream, Fig 1 1 The injected jet may also separate at the rear end of the slot and subsequently reattach producing a separation bubble Further downstream, there is turbulent mixing between the coolant film and the free stream Although, two-dimensional slot injections have been found to be very effective, these are rarely used for turbine blade cooling due to mechanical and thermal stress consideration with the possible exception of the trailing edge region One alternative to the slot injection is the injection from a row of discrete holes The flow field generated under these circumstances is no more two dimensional, but more complex three dimensional in nature until far away from the holes For an isolated jet, as the jet fluid leaves the hole, it retards the main flow along the upstream side of the jet causing an increased pressure there, whereas, rarefaction occurs at the downstream side The upstream high pressure causes a

bending of the injected jet and in certain cases a reverse flow behind the jet is formed due to low pressure in that region Owing to the shearing of the bending-over jet by the crossflow, a pair of contra-rotating vortices is generated, which lead to the secondary motion and consequently modify the jet cross sectional shape to a kidney-like from For ejection from a row of holes, each jet interacts with the neighbouring jets, with the mainstream and its boundary layer This interaction creates a layer of contra-rotating vortices, which develop into film cooling downstream of injection The flow topology corresponding to the discrete hole injection and the coolant layer formation is shown in Fig 1 2 The highly complex flow field created by the secondary fluid injection depends on a wide variety of influence parameters

Studies of film cooling have, for the most of the cases, focused on the geometric and fluid mechanical variables that control the heat transfer as the hot combustion gases form a boundary layers like flow over the surface and as the wall shear layer interacts with the cooling jets emerging at various locations along the surface Parameters that govern the jet-crossflow interaction and its associated surface heat transfer are both geometric hole shape, angle, spacing, and pattern, and fluid mechanical jet-to-crossflow ratios of density (DR), velocity (VR), mass flux or blowing (BR), and momentum flux (MR)

These ratios are defined as

$$DR = \frac{\rho_J}{\rho_\infty},\quad VR = \frac{V_J}{V_\infty},\quad BR = \frac{\rho_J V_J}{\rho_\infty V_\infty} \text{ and } MR = \frac{\rho_J V_J^2}{\rho_\infty V_\infty^2} \tag{1 1}$$

where, the subscripts ∞ and J refers to the fluid states of the cross flow in the free-stream and of the injectant at the location where it emerges into the cross flow

In jet-crossflow applications the wall heat flux, q'', is usually defined using an analogy to convective heat transfer with high speed flows, whereby an adiabatic wall temperature replaces the far field temperature of the cross flow (Goldstein, 1971),

$$q'' = h_f\,(T_{aw} - T_w) \tag{1 2}$$

In the equation (1 2), h_f is the convective heat transfer coefficient, T_w is the flat plate wall temperature and T_{aw} is the adiabatic wall temperature

The adiabatic wall temperature as a function of distance downstream of injection must be experimentally determined for a given film cooling geometry and cross flow hydrodynamics The data are generally presented non-dimensionally in terms of adiabatic film effectiveness, η_{ad}, defined as

$$\eta_{ad} = \left(\frac{T_\infty - T_{aw}}{T_\infty - T_j} \right) \tag{1 3}$$

where, T_j is the temperature of injected jet and T_∞ is the main stream temperature

For injection at the free-stream temperature, the adiabatic wall temperature becomes the same as the free-stream (and jet) temperature and hence the heat transfer coefficient can be found from the difference between the wall and free-stream temperatures (Eckert, 1984) It is clear that distributions of both the heat transfer coefficient and the adiabatic wall temperature are required to predict film cooling heat transfer

The net benefit from film cooling can be quantified as a *Net Heat Flux Reduction* (NHFR) due to film cooling, or the ratio of reduction in heat transfer to the blade with film cooling to heat transfer without film cooling The is similar to the Stanton number reduction described by Luckey, et el (1977)

$$NHFR = 1 - \frac{q''}{q''_o} = 1 - \left(\frac{h_f}{h_o} \right) \left(\frac{T_{aw} - T_w}{T_\infty - T_w} \right) \tag{1 4}$$

or,
$$NHFR = 1 - \left(\frac{h_f}{h_o} \right) (1 - \eta_{ad}\theta) \tag{1 5}$$

where,
$$\theta = \left(\frac{T_\infty - T_j}{T_\infty - T_w} \right) \tag{1 6}$$

The subscript 0 denotes conditions with no film cooling and *f*, with film cooling The objective of film cooling is to increase NHFR by increasing η_{ad} and reducing $\left(\frac{h_f}{h_o}\right)$ The ratio of convective heat transfer coefficient with and without film cooling $\left(\frac{h_f}{h_o}\right)$ depends on the boundary layer hydrodynamics of respective conditions The heat transfer coefficient with secondary injection is often assumed to be that which would exist for the same boundary layer hydrodynamics but no injection (dry wall condition), although it will deviate from the no-injection value in the near hole region This assumption leaves a majority of the film cooling research, to date, focused on the adiabatic wall temperature, and how it depends on the geometric and fluid mechanical parameters

1.3 Aim of the present investigation

The main objective of the present study is to experimentally determine the film effectiveness over a flat surface for different blowing and density ratios The relative hot secondary air is injected into the mainstream through a series of seven discrete holes in a row, inclined at an angle 35^0 with respect to the surface Another configuration was a skewed hole, having a compound angle of 60^0 with the streamwise direction in the *x-z* plane and an angle of injection of 35^0 as before The latter was used to examine the effect of compound angle to minimize the lateral variation of effectiveness in the near field region However, the compound angle may increase the losses and affect streamwise adiabatic effectiveness due to enhanced mixing created by a lateral induced velocity of injected jet Although for the present investigation, the loss calculation has not been looked upon As already noted, for the present experiment the expression for η_{ad} would be same even with hot secondary injection The values of hole spacing, length and injection angle were selected to be representative of gas turbine film cooling geometry to evaluate the film effectiveness over the plate surface All the measurements were taken at steady state condition

The experiment was performed at three blowing ratios, 0.5, 1 0, and 1 44 respectively The temperature ranges were varied from 40^0 to 60^0C, which resulted into a variation of density ratio in the range of 0 937 to 0 880 Velocity field was measured at 3 5*D* upstream of the blowing holes

to determine the nature of the approaching boundary layer Downstream boundary layers were also measured at x/D = 5 0, 10 0, and 15 0 to determine the formation of shear layer with injection Temperatures were recorded from the sensors placed along the centerline of the center hole and also along the line of symmetry between two adjacent holes for both the hole-configurations and have been presented non-dimensionally in terms of adiabatic film effectiveness (η_{ad})

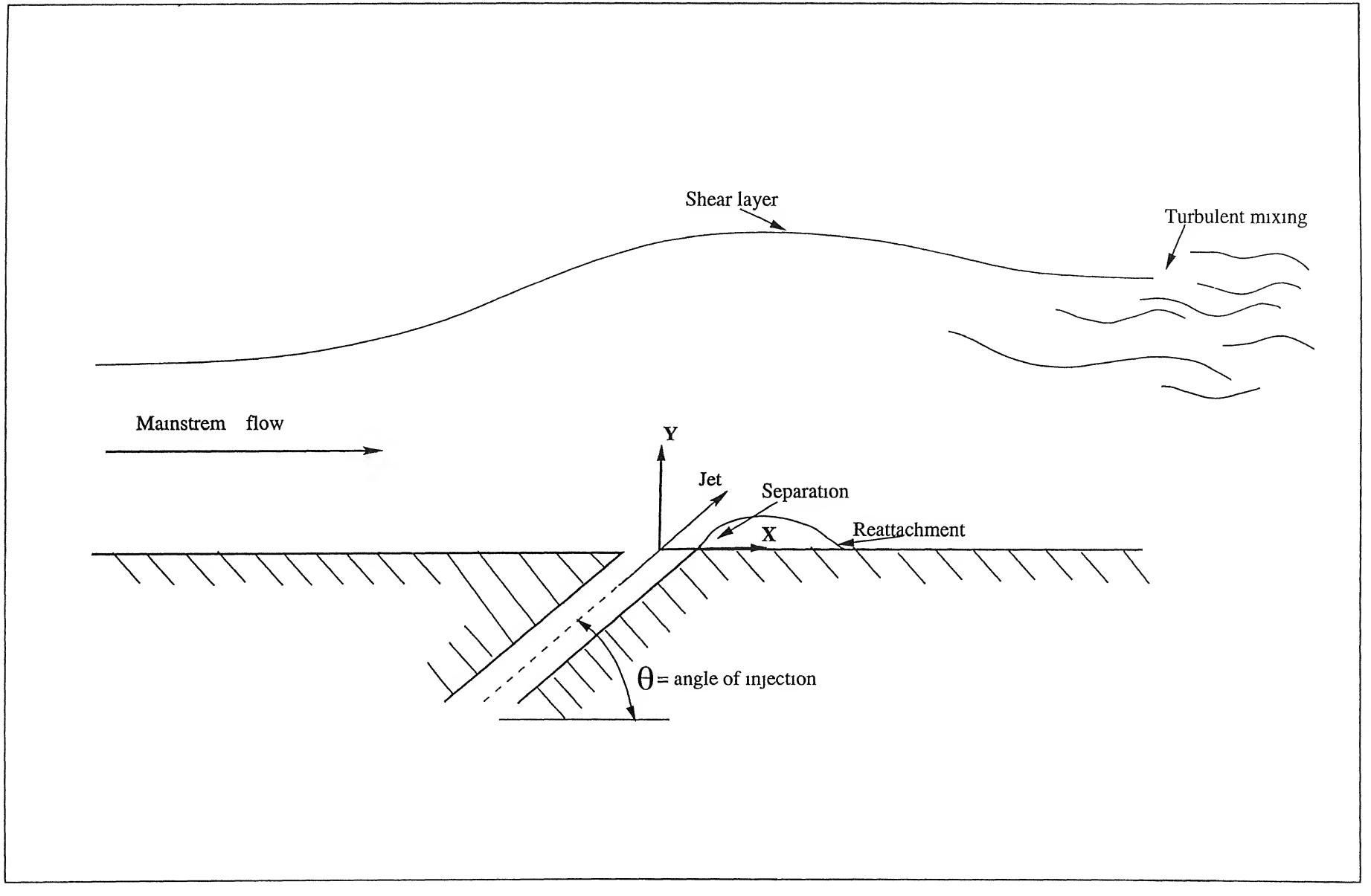

Fig. 1.1 Flow field for slot injection

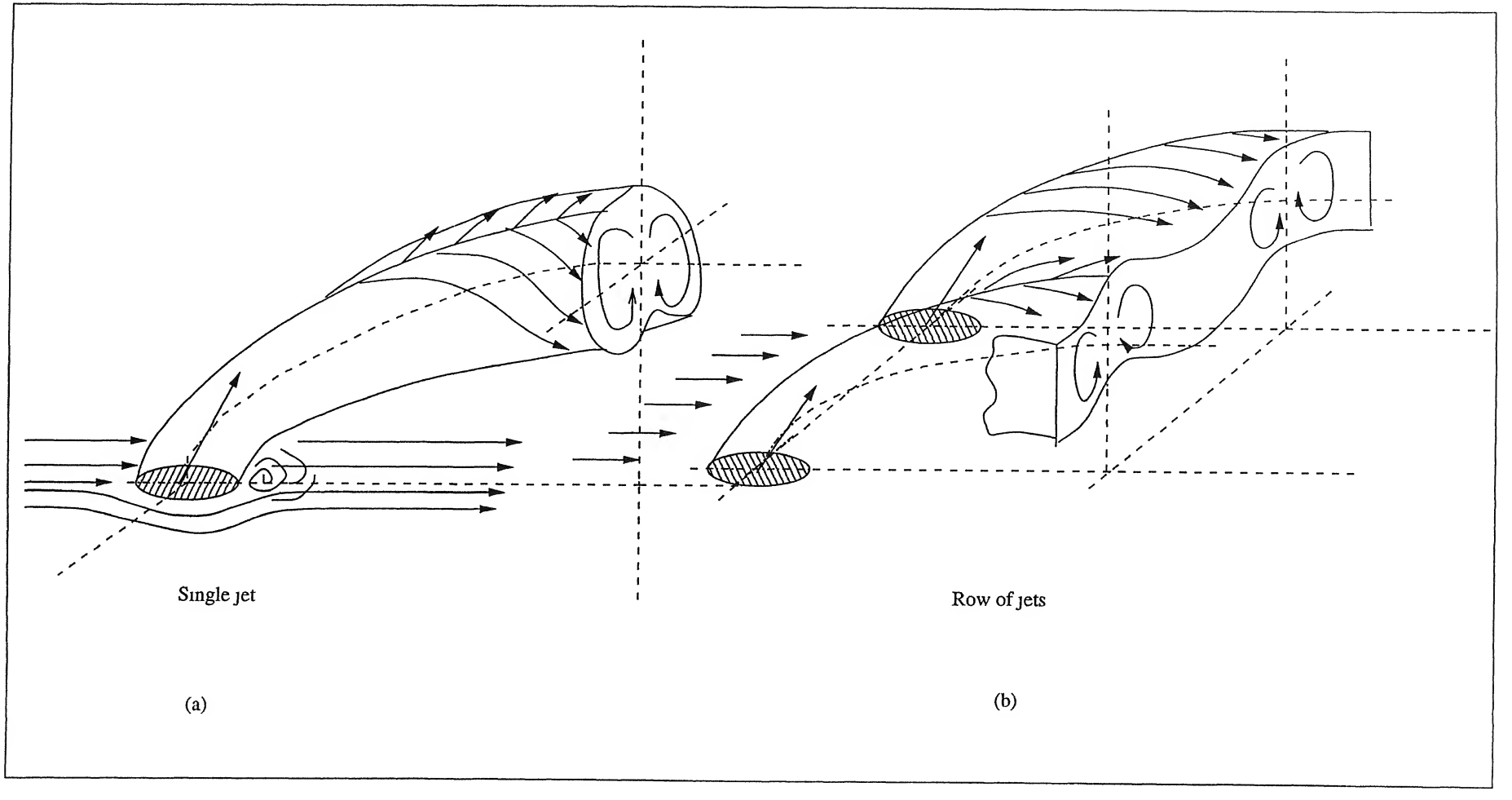

Fig. 1 2 Flow field for discrete jet injection

CHAPTER 2

LITERATURE REVIEW

A detailed review of literature, covering different aspect of jet-cross-flow interaction and film cooling associated with flow and heat transfer problem are presented in this chapter The major emphasis is given to the experimental techniques applied to flat plate geometry Along with flat plate technical literatures concerning the relevant aero thermal investigation on turbine cascade and curved surface are also surveyed in order to highlight the state-of-the-art

Both discrete hole film cooling and slot film cooling over a flat plate has been experimentally investigated extensively In general the experimental study on film cooling and jet-crossflow interaction can be subdivided into three categories, namely surface temperature and thermal characteristics measurements, parametric studies and aerodynamic investigation

One of the earliest works on three-dimensional film cooling was due to Goldstein et al [1972] In their experiment they studied film cooling downstream of secondary gas injection through discrete holes The influence of hole geometry, secondary fluid density, and main stream boundary layer thickness were described Significant improvements in the film cooling effectiveness were observed by having the secondary jet passages widened before the exit into the mainstream The experimental results indicated the improvement of three-dimensional film cooling which was obtained with shaped channels for the secondary flow This was due to the fact that the mean velocity of injection was decreased with larger exit area which resulted into lower effective blowing ratio and thus less jet penetration

The effect of large density difference on film cooling effectiveness was investigated through heat-mass transfer analogy by Pederson et al [1977] Experiments were performed in a wind tunnel where one of the walls was provided with a porous strip or a row of holes with three

diameter lateral spacing and inclined at 35° into the main stream Helium, CO_2, or refrigerant F-12 was mixed with air to approach constant property situation The density ratio was varied between 0 75 to 4 17 for both injection systems The study revealed that density ratio has a strong effect on the film effectiveness for injection through holes The film effectiveness for injection through holes had a maximum value for velocity ratio between 0 4 and 0 6 The centerline effectiveness increases somewhat with a decreasing ratio of boundary layer thickness to injection tube diameter

Detailed studies had been made by Foster and Lampard [1980] on effectiveness and flow downstream of a row of holes in the flat floor of a wind tunnel using a mass transfer technique The effects of variation of injection angle, upstream boundary layer, and hole spacing were described, and an assessment of the relative aerodynamic penalty was made The result showed that small injection angles give the best cooling effectiveness at low blowing ratio while large injection angles are best at high blowing rates The result also depicted that increasing upstream boundary layer has negative effect on effectiveness due to enhanced lateral mixing and film dilution, and small hole spacings give improved lateral coverage and alleviate jet lift-off effects

An experimental investigation of film cooling on a rough surface had been performed by Goldstein et al [1985] using a mass transfer technique Two injection geometries (one and two rows of holes) and six roughness patterns were used The presence of roughness causes a decrease in spanwise-averaged effectiveness for both injection geometries at low blowing rates, and an increase in the effectiveness for one-row injection at high blowing rates, but not for two-row injection The results for two-row injection (with or without roughness) can be correlated by a parameter used to correlate slot injection data The influence of roughness pattern on the average effectiveness and on the lateral uniformity of the effectiveness had also been described

Jurban and Brown [1985] performed extensive experimental work in film cooling effectiveness of two row of holes inclined in streamwise and spanwise directions The effects of hole and row spacings and combination of inclinations were investigated in the presence of free-stream pressure gradients and turbulence for a typical range of blowing rates It was obvious from the

result that the effect of increasing the distance between the two rows of holes had a detrimental effect on both local and averaged film cooling effectiveness downstream of the second row of holes for all blowing rates

Hay et al [1985] worked on the sensitivity of the heat transfer coefficient under the film to the state of approach boundary layer for injection through a row of holes on a flat plate For the same injection geometries, the effect of injection in the presence of mild adverse, mild favourable, and strong favourable mainstream pressure gradient was investigated The results indicated that the heat transfer coefficient under the film was sensitive neither to the condition of approach boundary layer nor to the presence of a mild adverse pressure gradient, but it was significantly lowered by the favourable pressure gradient, particularly at the low blowing ratio

Film cooling effectiveness was studied by Sinha et al [1991] using a row of inclined holes that injected cryogenically cooled air across a flat adiabatic test plate Density ratio was varied from 1 2 to 2 0 and surface temperatures were measured using a unique surface thermocouple arrangement, free of conduction error Temperatures were obtained along the jet centerline and across a number of lateral locations By independently varying density ratio and blowing rate, scaling of adiabatic effectiveness with mass flux ratio, velocity ratio, and momentum ratio was determined Laterally averaged effectiveness was found to be dependent on density ratio and momentum flux ratio Decrease in density ratio and increase in momentum flux ratio were found to reduce the spreading of the film cooling jet significantly and thereby reduce laterally averaged effectiveness

F Lo′pez Peña and T. Arts [1992] experimentally investigated different aerodynamic aspects of the flow field generated when a single jet or a row of jets are ejected into a mainstream The similarity parameters were taken such as to match those of the 3D film cooling The study was made on three different models installed in a low speed wind tunnel The first model was a flat plate with a single inclined circular hole, the other two models presented the same configuration but with different row of holes at different pitch-to-diameter ratio in each case The flow field was studied by means of an LDV system The vortex pair generated within a single jet

appeared to have a trend towards separation some diameters after the injection location In case of a row of jets, the interaction between the jets lowered the height of jet penetration The momentum flux ratio is found to characterized the interaction between jet and incoming boundary layer When the momentum flux ratio was lower than 1 0, the jet penetration was small, and the jet was essentially confined within the boundary layer

Experiment was performed by Ligrani et al [1992] to investigate the development and structure of flow downstream of one row and downstream of two staggered rows of film cooling holes of compound angle orientation Results presented include distribution of iso-energetic Stanton numbers, and adiabatic film cooling effectiveness deduced from Stanton numbers using superposition Also presented were plots showing the streamwise development of injectant distributions and streamwise development of mean velocity distribution Spanwise-averaged values of the adiabatic film cooling effectiveness, $\overline{\eta}$, measured downstream of two staggered rows of holes were highest with a blowing ratio of 0.5, and decrease with blowing ratio because of injection lift-off effects for x/d<20

Honami et al [1994] described the behaviour of the injected jet on the flat surface in lateral injection of film cooling Simultaneous velocity and temperature measurements were made by the double wire probe The test surface was also covered with an encapsulated temperature-sensitive liquid crystal The image processing system, based on the temperature and hue of the liquid crystal calibration, provided the surface temperature distributions The tests were conducted at three mass flux ratios, 0 5, 0 85, and 1 2 The laterally injected jet had an asymmetric structure with a large scale of vortex motion on one side caused by the interaction with the primary stream Asymmetry was promoted as mass flux ratio is increased resulting in low film cooling effectiveness

Sen et al [1996] measured heat transfer coefficient for film cooling injection from a single row of holes of different configurations The experiment was conducted at a density ratio of 1 0 The results were presented in terms of the ratio of film cooling heat transfer coefficient to the heat transfer coefficient for undisturbed turbulent boundary layer at the same location Results

indicated that for the streamwise directed holes, the heat transfer rates were close to the levels that existed without injection Similarly, at low momentum flux ratio, holes with a large compound angle had little effect on heat transfer rates However, at high momentum flux ratios, holes with a large compound angle had significantly increased heat transfer levels The results were combined with adiabatic effectiveness results to evaluate the overall performance of the three geometries Compound angle injection at high momentum flux ratios gave higher effectiveness values than streamwise directed holes, but the higher heat transfer levels resulted in poorer overall performance

The film cooling performance and velocity fields were investigated by Kohli and Bogard [1997] for discrete round holes with relatively large injection angle of 55° Results were compared to typical round film cooling holes with 35° injection angle All experiments were in this study were performed at a density ratio of 1 6, using cryogenically cooled injectant. Thermal field and two component mean velocity and turbulence intensity measurement were made Injection at large angle showed only a slight degradation of centerline effectiveness for low momentum flux ratios, while a significant reduction in effectiveness was seen at higher momentum flux ratios The thermal field of 55° round holes indicated a faster decay of cooling capacity than that of 35° holes

Goldstein and Stone [1997] presented film cooling effectiveness data against a backdrop of ammonium-diazo flow visualizations for row of holes injection along a convex wall and a concave wall at angles of 15^0, 25^0, and 45^0 to the mainstream and density ratios of approximately one and two The condition of the local boundary layer, the severity of jet lift-off, and the strength of vortex interactions among the bound vortices of neighbouring jets were key considerations in interpreting the data On both the concave and convex walls the film cooling effectiveness was directly related to rate of injection The effectiveness increased with increase in the blowing ratio upto the lift-off value (the value of blowing ratio at which the jets lift away from the wall) but beyond that it decreased substantially

Ligrani, and Ramsey [1997] studied the adiabatic effectiveness and iso-energetic heat transfer coefficient from the measurements downstream of film cooling holes inclined at 30° with respect to the surface in lateral planes With this configuration, holes were spaced 3D apart in the spanwise direction and 4D in the streamwise direction in two staggered rows Results were presented for an injectant to freestream density ratio near 1 0, and injection blowing ratio from 0 5 to 1 5 The result showed that spanwise-averaged adiabatic effectiveness values are significantly higher for two-row staggered holes than the values measured downstream of a single row of holes

Jabbari et al [1996] performed film cooling experiment for injection through discrete holes in the endwall of a turbine blade The effectiveness was measured at 60 locations in the region covered by injection Three nominal blowing rates, two density ratios, and two approaching flow Reynolds numbers were examined Analysis of the data revealed that even 60 locations are insufficient for the determination of the field of film cooling effectiveness with its strong local variations Visualizations of the traces of the coolant jets on the end wall surface, using ammonium-diazo-paper provided useful qualitative information for the interpretation of the measurements, revealing the paths and interaction of the jets, which change with blowing rate and density ratio

Fredrichs et al [1997] investigated the aerodynamic aspects of endwall film cooling, in which the flow field downstream of a large-scale low-speed linear turbine cascade had been measured The integrated losses and locations of secondary flow features with and without secondary endwall film cooling had been determined for variations of both the coolant supply pressure and injection location The result revealed that it was necessary to take the three dimensional nature of the endwall flow into account while designing the endwall film cooling configurations

Turbine blade endwall heat transfer measurements were presented by Giel et al [1998] for a range of Reynolds and Mach numbers Data were obtained for Reynolds numbers based on inlets conditions of 0 5 and $1\,0\times 10^{6}$, for isentropic exit Mach numbers of 1 0 and 1 3, and for free stream turbulence intensities of 0 25 and 7 0 percent Test were conducted in a linear cascade at

the NASA Lewis Transonic Turbine Blade Cascade Facility The result showed that the flow fields were highly three-dimensional in the cascade as a result of thick boundary layers at the test section inlet Endwall heat transfer data were obtained using a steady-state liquid crystal technique

Measurements of discharge coefficients for several film cooling configurations with hole length-to-diameter ratios of 2 3, 4 6, 6 6, and 7 0 were presented by Burd and Simon [1999] Discharge coefficients were discussed in terms of distribution of velocity and the effects of the hole supply plenum geometry The results revealed the influence of hole length and coolant supply geometry on the discharge coefficient Shorter film cooling holes had higher discharge coefficient due to greater interaction with the free stream

The survey of literature reveals that experimental investigations on film cooling have reached a level of maturity to illustrate the aero-thermal behaviour of coolant jets in hot cross flow over a flat plate as well as over a turbine cascade Although, relatively few investigations have been carried out to emphasize the understanding of aerodynamic aspect related to jet-crossflow interaction and coolant layer formation The present review has made an attempt to highlight the recent trend in the experimental research in the field of turbomachinery film cooling

CHAPTER 3

TEST SET UP AND INSTRUMENTATION

3.1 Introduction

In the middle of 1998, a plan was chalked out to develop a *variable inlet temperature* wind tunnel in the Energy Conversion Laboratory of IIT Kanpur for the investigation of aerodynamic and heat transfer aspects of film cooling over a flat plate and cascade geometry This project was started primarily as the experimental set up for an M Tech thesis work but also with a view to provide a new test facility for U G. experimentation in future Figure 3 1 shows the overall view of the test set-up Different parts of the test set up with specific features are described below

3.2 Description of the test set-up

The total set-up has been divided into two major parts main tunnel and secondary blowing loop One end of the main tunnel is attached to the settling tank and the other end is free to the atmosphere The settling tank with the axial fan unit was already installed For ease of fabrication the main tunnel is subdivided into several modules as mentioned below

- Entrance section and provision for mainstream air heating
- Flow straightener section
- Convergent section
- Test section
- Divergent exit section

Similarly, the secondary unit consists of the following components

- Suction chamber and connecting flexible pipes
- Blower
- Secondary heater
- Plenum chamber for blowing

Different instruments and sensors used in the experiment are

- Temperature sensor (*PRTD*100)
- Pitot tube
- Orifice meter
- Manometers (U-tube and Inclined tube)
- Temperature recorders

3.2.1 Main tunnel

The atmospheric air is sucked by a two stage axial flow fan which is driven by a motor of 7 5 kW capacity The speed of the motor and thus the fan speed can be controlled by a thyristor control unit The fan is connected to the settling tank through a duct, which helps to settle the flow before it enters the main tunnel section For the present work, the remaining part beyond the settling tank has been fabricated The test set-up has been fabricated from 1 9 mm thick cold rolled MS sheet and flanges were made from 50mm× 6mm cold rolled flat Figure 3 1 shows the schematic and Fig 3 2 the photograph of the main tunnel

The entrance from the settling tank to the main tunnel is made beveled to reduce the entrance loss and to avoid flow separation One end of the section is 25″×25″ and the other end is 20″×20″ Next part is a 16″ long 20″×20″ square section where provision is kept for placing heaters within the tunnel to heat the mainstream air

The next part on the downstream side is also a 20″×20″ square section with a flow straightener placed inside Length of the section is 16″ and the last 6″ is occupied by the flow straightener mesh The grid size of the mesh is 2″×2″ square and length of the straightener is 6″ It was fabricated separately and placed inside the section The flow straightener is followed by a convergent section, which reduces the tunnel section from 20″×20″ to 20″×6″ The change in cross section is gradual with a contraction cone angle $2\theta \approx 60°$, and length of the section is 12″ This contraction would further damp down the flow fluctuation or oscillation, if any The smaller end of the convergent section (which is connected to the test section) was made 20" × 6" i e larger

width than its height, considering the fact that the approach boundary layer would be two dimensional

Most important part of the tunnel is the test section It is 59″ (1 5 meter) long and cross-sectional area of 20″×6″ The bottom surface holds a suction chamber for sucking air below the leading edge of test plate and a plenum chamber for blowing of secondary air The test plate is bolted at the bottom surface and slot has been cut to make room for PRTD wires One of the side walls has several pressure taps for static pressure measurement along the streamwise direction The other side has one temperature tap for measuring mainstream temperature (ahead of blowing holes) and a hinged door for inserting a section of the test plate with injection port inside the tunnel The door has rubber lining on the periphery to prevent any leakage during experiment The top roof of the test section has a large window for fixing the three-dimensional probe traversing mechanism The outside surface of the test section was covered by low conductivity black foam to reduce the conduction losses The last part is a 12″ long divergent exit section with an angle of divergence $2\alpha = 20°$ All the modules of test section are connected sequentially by bolts and gaskets have been placed between the flanges to prevent leakage of air

3.2.2 Secondary blowing circuit

In the experimentation of jet–crossflow interaction a secondary blowing circuit is always required to create an injectant jet into the mainstream A small blower of 1 7 m^3/min discharge capacity was used for blowing and leading edge suction, Fig 3 1 Both the blowing and suction were controlled by means of three butterfly type of valves. The suction end of the blower is connected to the atmosphere as well as the leading edge suction chamber through a *tee* joint and flow through the pipelines were regulated by the valves The discharge end is connected to the heater and in between one blow-off valve has been placed to check the flow towards plenum chamber An orifice meter was placed in between the plenum chamber and secondary heating unit to measure the volume flow rate of blowing Figure 3 3 indicates the photograph of the secondary blowing circuit

The capacity of the secondary heater is 5 kW Five cylindrical heating rods, each of which can generate 1 kW heat, were used for heating the secondary blowing air The heating rods were placed inside a closed chamber The heater has been designed in such a way that we can optionally use 1-5 kW at a time according to the requirement An orifice meter was used in the blowing circuit to measure the flow of hot blowing air

The secondary blowing circuit has distinctly two zones one cold region and another hot region The pipelines and apparatus placed before the inlet of the heater are in the cold region and those on the downstream of the exit of the heater fall in the hot region PVC pipes were used for cold region and asbestos impregnated synthetic rubber pipes were selected for the hot pipelines to sustain the temperature of hot gases and minimize the heat loss to atmosphere

3.2.3 Test plate

The test plate consists of three different sections, a 20 cm long leading edge plate with 45^0 leading edge angle, followed by an insertable type injection hole plate of 10 5 cm length The injection plate is followed by an adiabatic instrumented plate The test plate assembly is shown by Fig 3 4 For the present study, a single row of seven holes with two types of hole geometry was used Both the hole-configurations have 35^0 inclination angle with respect to the surface One set of holes is parallel to the streamline and other one is having a compound angle, CA = 60^0 with the stream wise direction Figure 3 5 indicates the photograph of different hole configurations

The diameter of the hole D=10 mm, length L=4 5D and spacing P=3D This configuration is representative of the actual gas turbine film cooling geometry Hole inlet and exits are sharp edged and the interior surfaces of the holes are aerodynamically smooth The test hole plate can be inserted from the side door of the test section wall This was designed to conveniently use different type of hole configuration without replacing the whole test plate Leading edge plate and instrumented plates are bolted to the inner bottom surface of the test section and test hole plate can be placed between them by sliding through the door The sliding surfaces of the test hole plate are beveled at 10^0 angle to retain the plate in proper position during blowing of secondary air

The instrumented downstream plate is 89 5 cm long, temperature sensors have been placed along the centerline of the center hole and the line of symmetry between the two holes from 2*D* to 50*D* at 34 locations Special material (*polyglas*) of very low thermal conductivity, was chosen for making an approximately adiabatic test plate The properties of the material are given in the Table 3 1 Thickness of the test plate is 25 mm The bottom part of the test plate, exposed to the atmosphere has been covered by 6 mm thick black foam to prevent backside conduction losses

Table 3 1 Properties of the *polyglas*

Physical properties	**Value**	**Unit**
Heat distortion temperature	85	^{0}C
Coeff. of thermal conductivity	0 01-0 02	Watt/m K
Coeff of thermal linear expn	7×10^{-5}	/^{0}C
Maximum recommended continuous service temp	80	^{0}C

3.2.4 Probe traversing mechanism

In our experiment, we measured the velocity profiles at various *x/D* locations For accessing any spatial location in the flow field, a simple mechanism was adopted by which the tip of the probe can easily be place at any desired location

The traversing mechanism has two parts

- Sliding plate traverse by which the probe can move in x- and z-directions
- Traverse gear this part enables the probe to move in y-direction and also to rotate

Figure 3 6 (a) and (b) depicts the schematic view of the sliding plate traverse along with the photograph of traverse gear

3.2.4.1 Sliding plate traverse

This part consists of three elements a fixed plate with a longitudinal window of width equal to the maximum crosswise travel of the probe, a sliding plate with a narrow slot of width equal to the diameter of the probe and length equal to the maximum lengthwise traverse of the probe, and a sliding block with a hole equal to the diameter of the probe at the center The mechanism is shown in Fig 3 6 (a)

The fixed plate is bolted at the opening on the roof of test section The sliding plate moves on the fixed plate along two guide ways to traverse in z direction and the block slides on the sliding plate along two longitudinal guide ways to traverse in the x direction Scales were fixed on the guide ways to measure the movements of the sliding elements The plates were made of 6mm thick *polyglas* and the block is 12mm thick This mechanism as explained above, provides a simplest way to traverse the probe in x-z plane

3.2.4.2 The traverse gear

The traverse gear was used to move the probe in y-direction The probe can also be rotated by this mechanism The linear movement in the y-direction can be measured from a fixed linear scale and a sliding vernier scale Thus the assembly of sliding plate traverse and the traverse gear made it possible to place the probe at any desired location within the flow domain

3.3 Instrumentation

As already explained, the objective of this work is to estimate the jet-crossflow interaction and also to evaluate the adiabatic film effectiveness over a flat plate surface for different blowing and temperature ratios, and hole configurations Thus, it has been decided to measure the velocity field created by the jet in crossflow and the surface temperature over an insulated flat plate

3.3.1 Temperature sensors

Most of the experiments done so far used thermocouples to sense the temperature For the present case, it has been decided to use highly accurate *platinum resistance temperature detector* (PRTD) to sense the local surface temperature PRTDs have been preferred over common thermocouples due to its higher stability, accuracy, and more linear resistance-temperature characteristics Figure 3 7 compare the resistance-temperature characteristics between thermocouple and RTD The PRTD used in our experiment is designated as PRTD100, uses a platinum helix threaded through a ceramic cylinder and affixed via glass-frit These devices maintain excellent stability in moderately rugged vibrational applications A metallic cap is fixed at the tip of the sensor to protect it from damage as shown in the photograph (Fig 3 8)

The RTDs were placed at 34 locations on the test plates along the centerline of the center hole and the line of symmetry between two holes They were inserted inside the drilled holes from the bottom side of the plate and then fixed flush with the top surface of the plate by applying adhesive and filler material to avoid any flow disturbance due to protruded portion above the surface The layout of the RTDs are shown in Fig 3 9

Before experimentation, the accuracy of the RTDs along with the temperature recorders were tested in a *distilled* water bath for three different temperatures (range 20^0 to 100^0C) within the range of operating conditions of the experiment The Appendix - A indicates the temperature of water recorded by different sensors and the corresponding water bath temperature measured by a glass thermometer (electronic thermometer for some cases) From the different charts in Appendix - A, it can be inferred that the maximum error in the temperature measurement of the RTDs along with the recorders i e , the whole temperature measurement system is about 2%

3.3.2 Temperature recorder

Multi point digital temperature recorder were used to record the temperature sensed by the PRTDs Two 10 point and two 8 point temperature recorders were used for measuring

temperature of 36 locations in the experiment Fig 3 10 shows the photograph of the temperature recorder

3.3.3 Pressure measuring instrument

Simple manometers were used for measuring the pressure in different regions of the test set-up U-tube manometers were used to measure the pressure difference across the orifice plate *Dwyers* inclined tube manometers (Range 1 0″ of water column) was used to measure the pressure from the boundary layer probe Tunnel mean pressure was tapped from the sidewall and used as a reference pressure for the boundary layer measurement *Dwyers* single column vertical tube manometer (Range 10 0″ of water column) was employed to get the static pressure head from the plenum chamber

3.3.4 Orifice meter

Orifice meter is preferred to flow nozzle or venturi meter for measuring flow through a duct because of its simplicity, ease of installation or replacement and low manufacturing cost Although, it has got the disadvantage of non-recoverable head loss, it is widely used as a flow-measuring device An orifice meter was designed and fabricated to measure the volume flow rate of secondary air in terms of difference in the of height of water column measured by an U-tube manometer The dimension has been selected in such a way that the *discharge coefficient* falls in the common range of 0 62 to 0 63 It was made of GI pipe and the orifice plate was made from 2 *mm* thick aluminium plate Downstream half of the orifice has been beveled at 60° to meet the actual design criteria, as illustrated in Fig 3 11

The principle of orifice meter is based upon the *Bernoulli Obstruction Theory*, the flow in the basic duct of diameter D is forced through an obstruction of diameter d, the ratio β of the device is a key parameter

$$\beta = \frac{d}{D} \qquad (3\ 1)$$

After leaving the obstruction, the flow may neck down even more through a *vena contracta* of diameter $D_2 < d$ Applying Bernoulli and continuity equations for incompressible steady frictionless flow to estimate the pressure change $(p_1 - p_2)$ as

Continuity $$Q = \frac{\pi}{4} D^2 V_1 = \frac{\pi}{4} D_2^2 V_2 \tag{3 2}$$

Bernoulli $$p_o = p_1 + \frac{1}{2}\rho V_1^2 = p_2 + \frac{1}{2}\rho V_2^2 \tag{3 3}$$

Eliminating V_1, we solve these for V_2 or Q in terms the pressure change $(p_1 - p_2)$

$$\left(\frac{Q}{A_2}\right) = V_2 \approx \left[\frac{2(p_1 - p_2)}{\rho\left(1 - D_2^4/D^4\right)}\right]^{1/2} \tag{3 4}$$

But this is surely inaccurate because we have neglected friction in a duct flow, where the friction will be very important We also do not want to get into the business of measuring *vena contracta* ratios D_2/d for use in equation (Eq 3 4) Therefore, we assume that $D_2/D \approx \beta$ and then calibrate the device to fit the relation,

$$Q = A_t V_t = C_d A_t \left[\frac{2(p_1 - p_2)/\rho}{1 - \beta^4}\right]^{1/2} \tag{3 5}$$

where, subscript t denotes the throat of the obstruction The dimensionless *discharge coefficient*, C_d, accounts for the discrepancies in the approximate analysis For our experiment, diameter of the pipe $D = 42\ 5$ mm, $\beta = 0\ 6$, $Re_d = 0\ 47 \times 10^5$, and $A_t = 5\ 10705 \times 10^{-6}\ m^2$

Thin plate orifice has been used with a plate thickness of $0\ 05D$ [28] The upstream side pressure tapping is at D distance and that on the downstream side is at $\frac{1}{2}D$ distance from the centerline of the orifice From the Fig 3 12, for $Re_d = 0\ 47 \times 10^5$ and $\beta = 0\ 6$, the value of C_d is

0 62 If the pressure difference is expressed in terms of height of water column Δh in *mm*, then the expression for volume flow rate Q becomes

$$Q = C_d A_t \left[\frac{2(\Delta h) \times 10^{-3} \times \rho_{water} \times g}{\rho_{air} \times (1 - \beta^4)} \right]^{\frac{1}{2}}$$

Or,
$$Q = 1\ 50332 \times 10^{-3} \sqrt{\frac{\Delta h}{\rho_{air}}}\ m^3/s \qquad (3\ 6)$$

3.3.5 Secondary heater

A heater of maximum capacity 5kw was used to heat the secondary blowing air The heater was designed to operate at various ranges between 1 to 5 kW in order to control the temperature of the blowing air Five heating coils have been placed inside a closed chamber with inlet and exit opening for air The chamber was insulated from inside to minimize the heat loss The heating coils are oriented in a zigzag fashion for maximum heat transfer to the secondary air, as shown in Fig 3 13

3.3.6 Blower

A constant speed small centrifugal blower (make *kpt*) of maximum discharge capacity 1 7 m^3/min was used for blowing and leading edge suction It was connected to the suction and blowing lines by means of two rubber nozzles, which fit in the grooves at the ends of the blower Flexible heat resistant pipes were used for the secondary blowing circuit

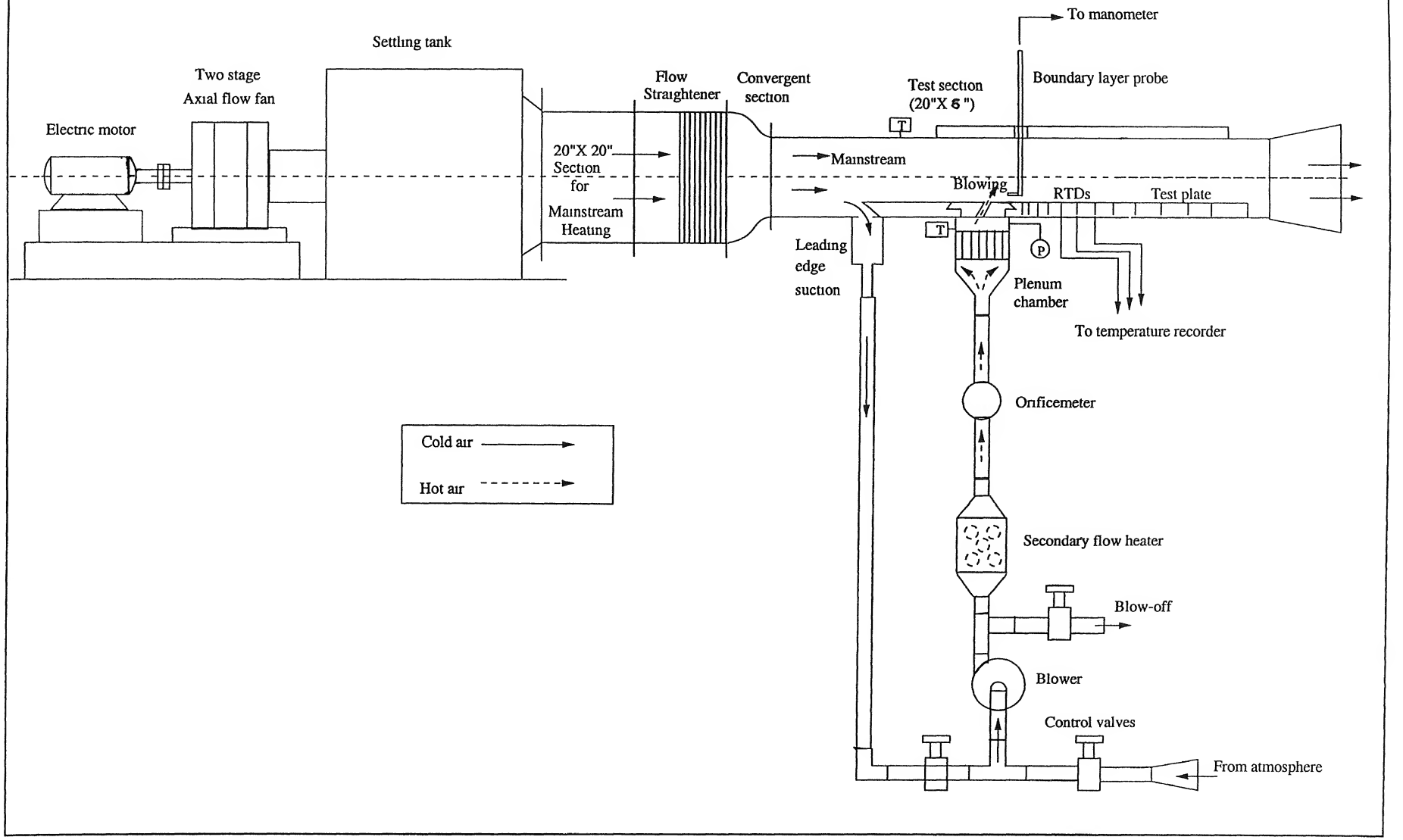

Fig 3 1 Schematic view of the test set up

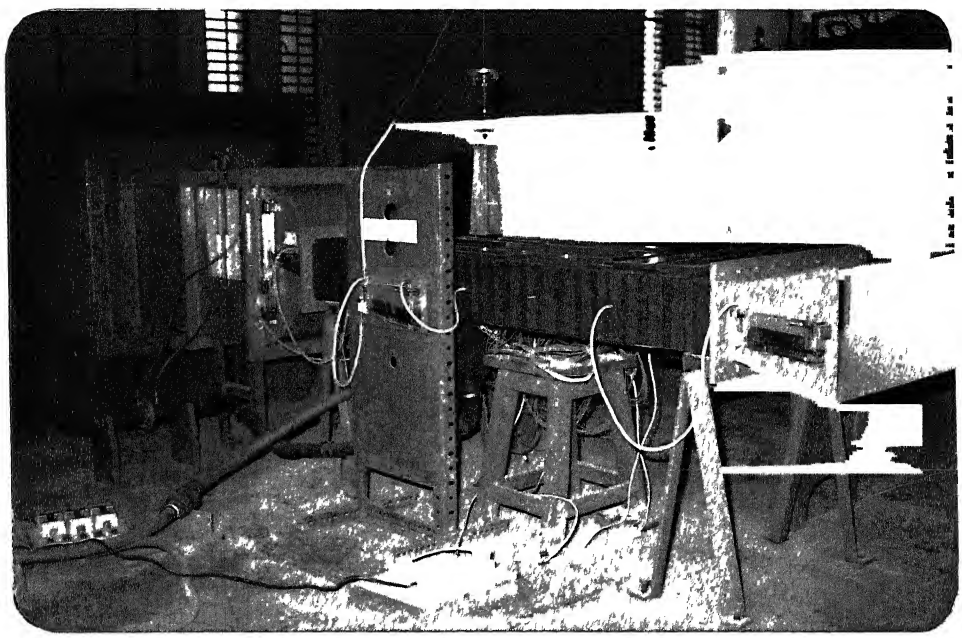

Fig 3 2 Photograph of the main tunnel

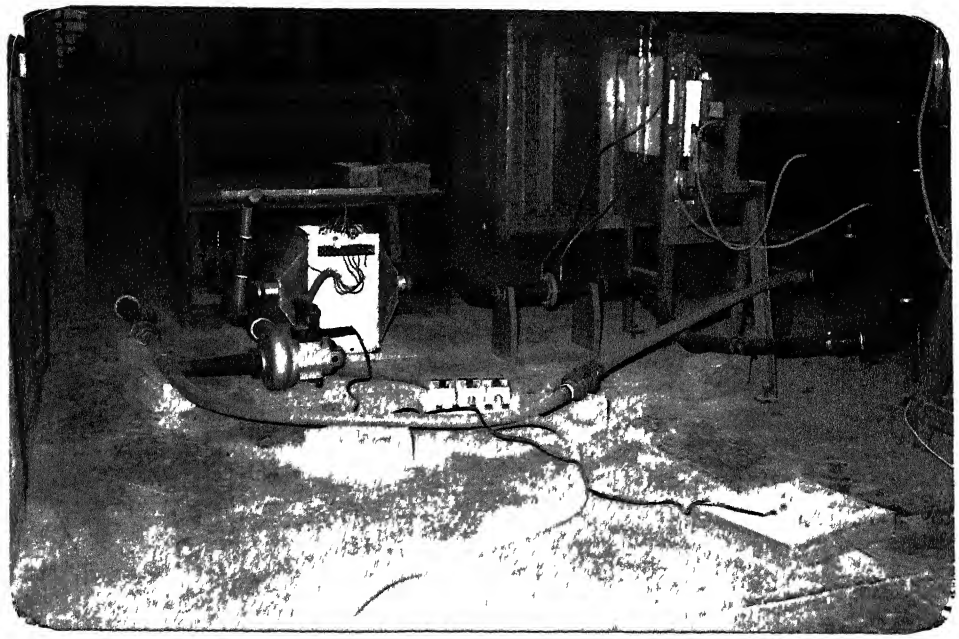

Fig 3 3 Photograph of the secondary blowing circuit

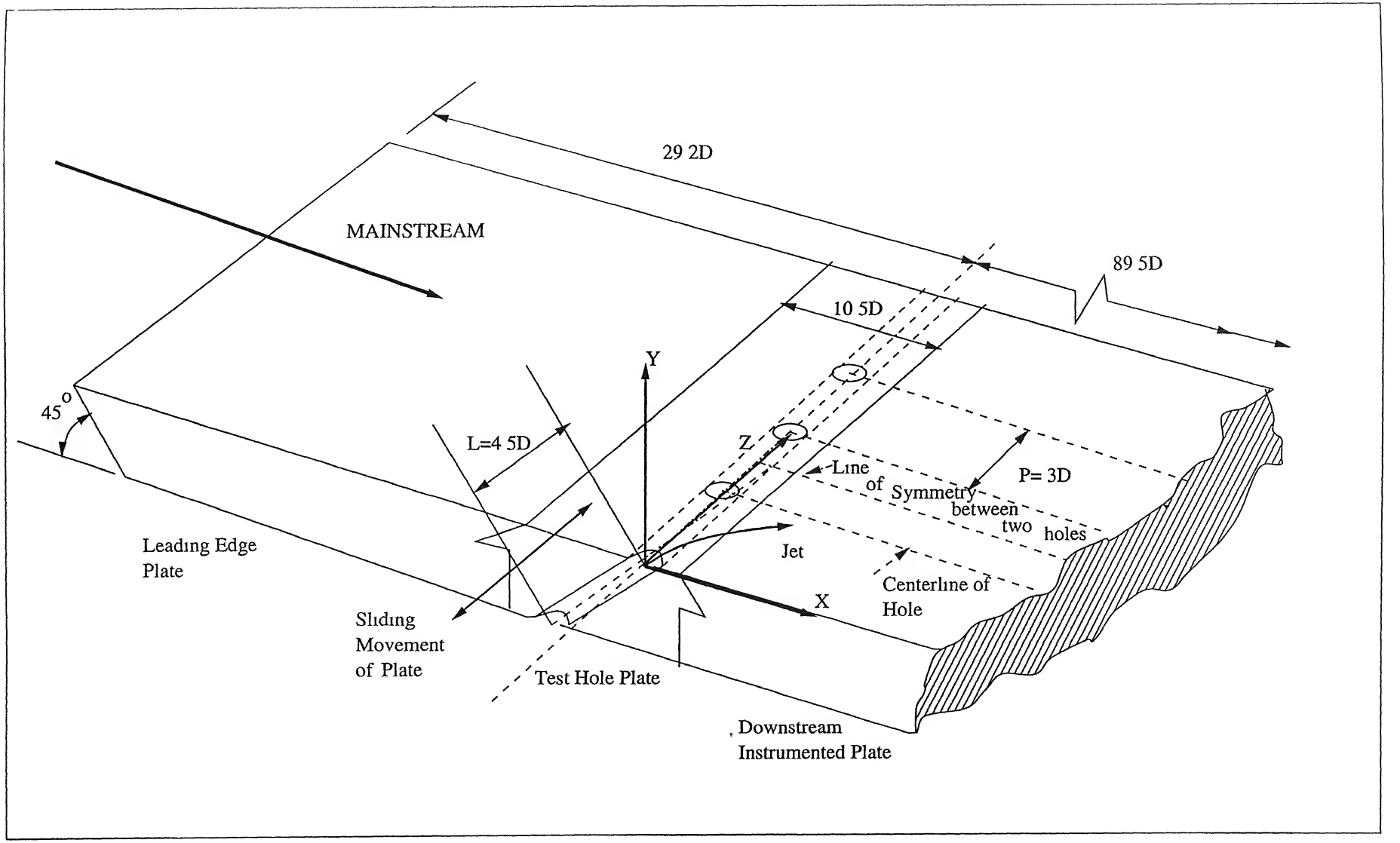

Fig 3 4 Schematic view of the test plate

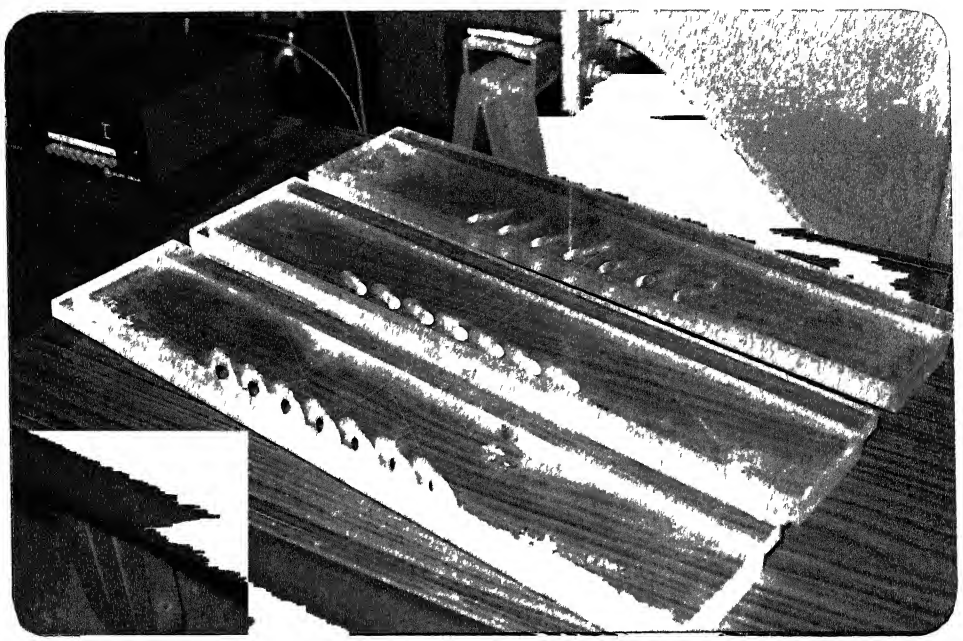

Fig 3 5 Photograph of different hole-configurations on the test plates

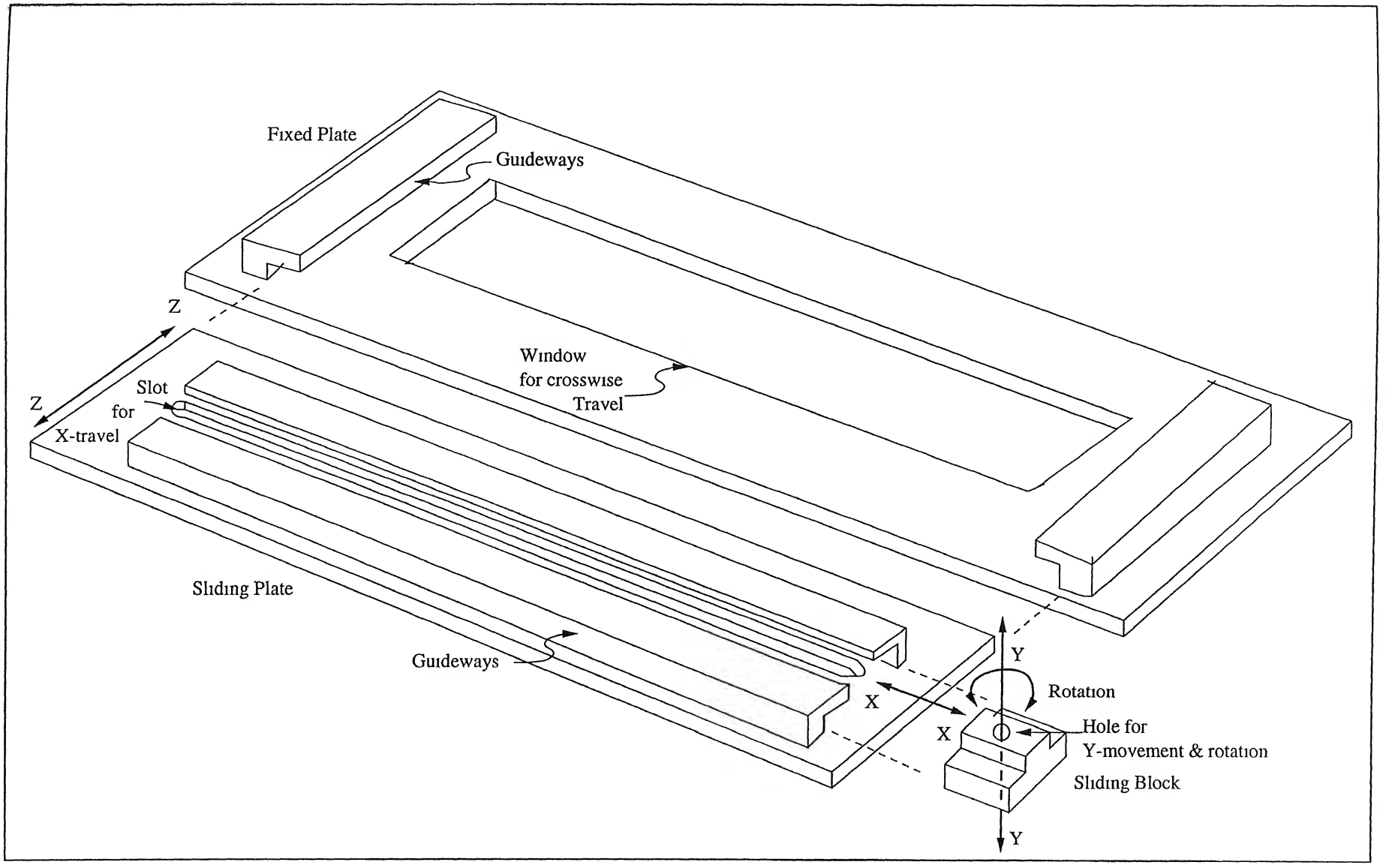

Fig 3.6(a) Probe traversing mechanism for streamwise and crosswise movement

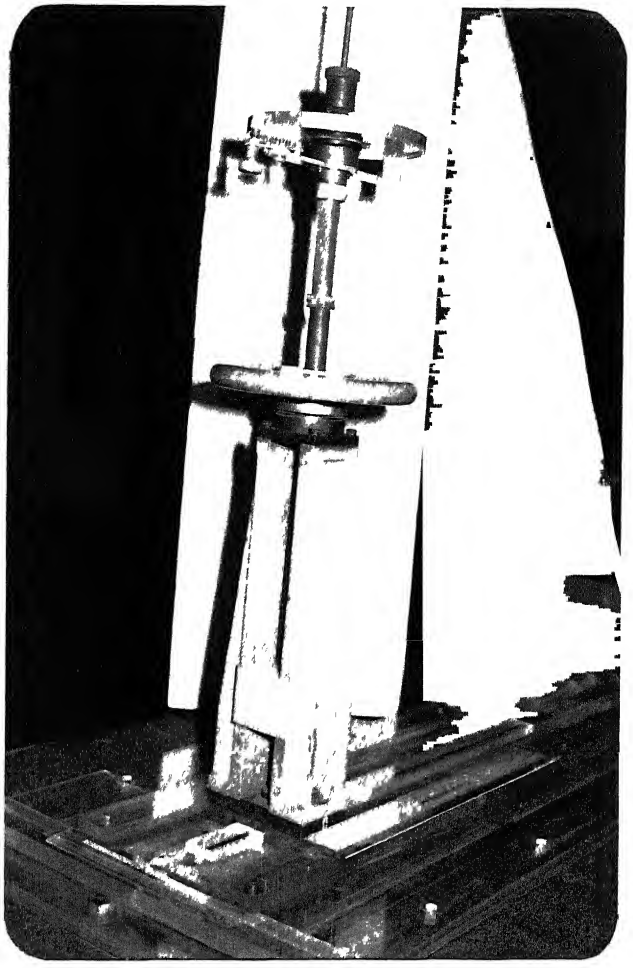

Fig 3 6(b) Traverse gear mechanism

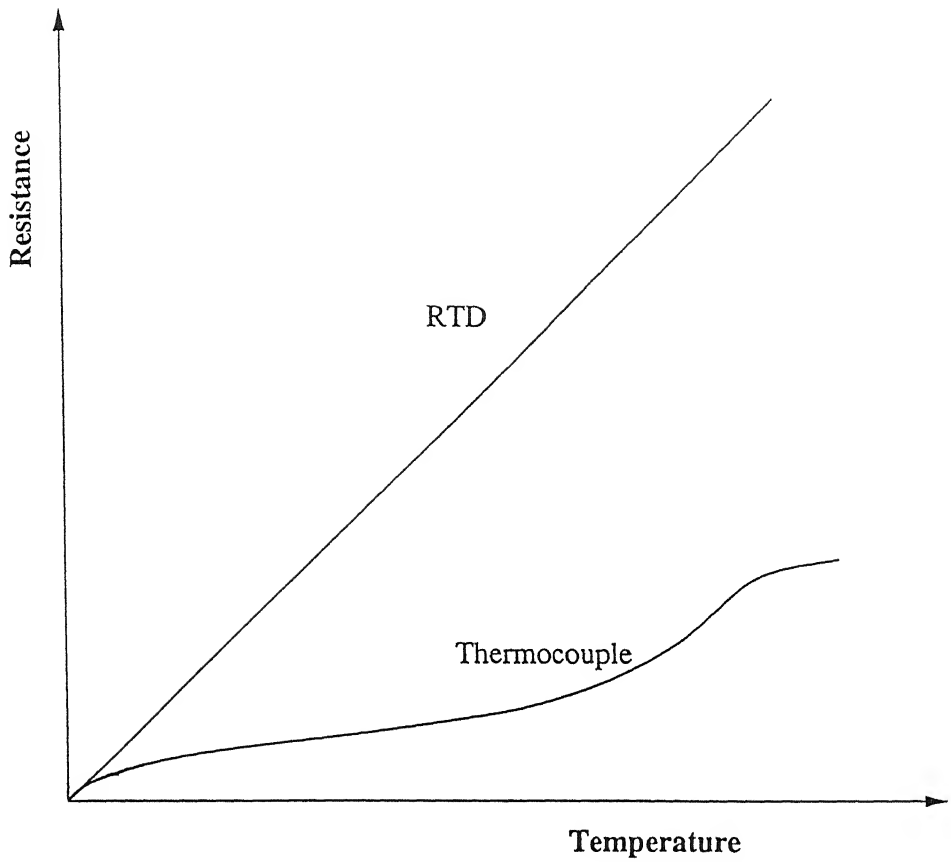

Fig.3.7 Resistance-temperature characteristics of RTD and thermocouple

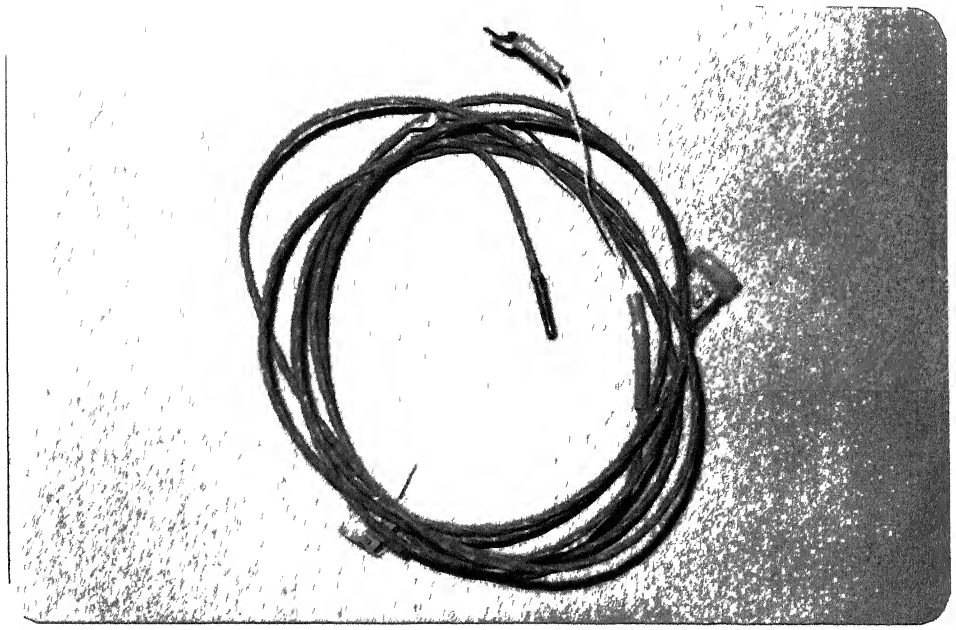

Fig 3 8 Photograph of the *PRTD*100

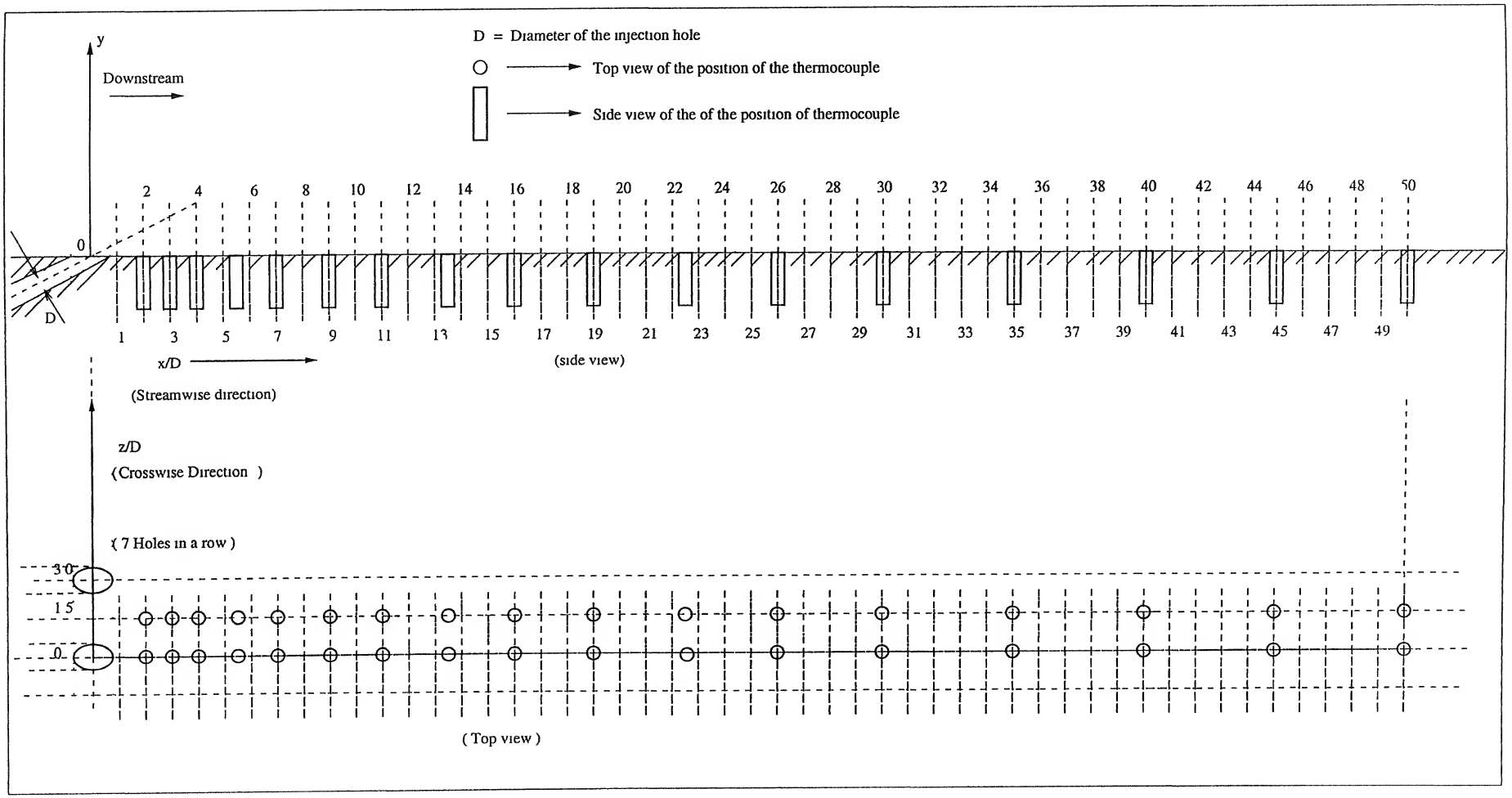

Fig 3 9 Lay-out of RTDs on the test plate

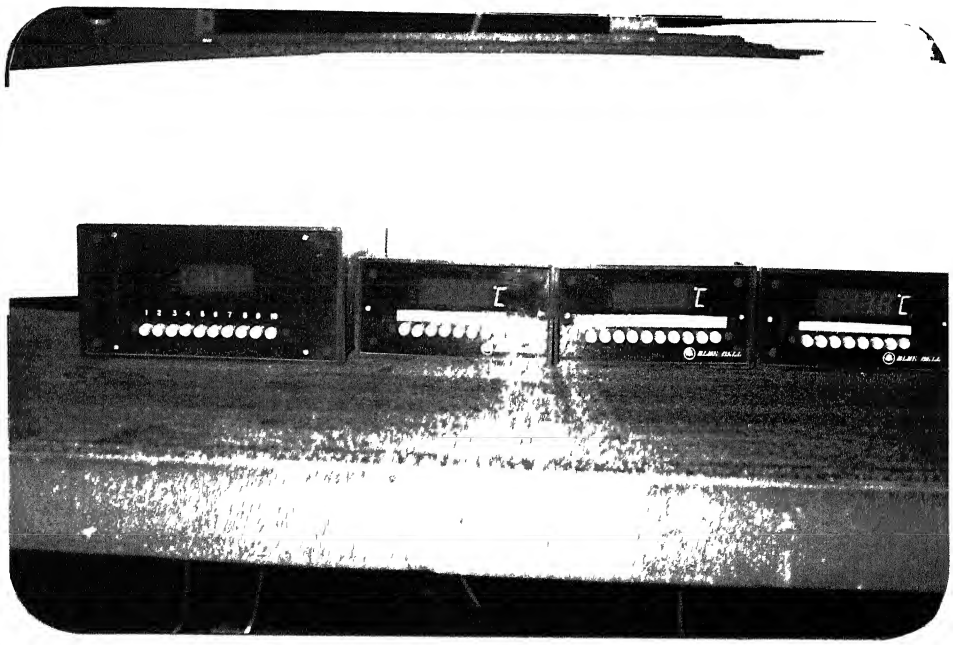

Fig 3 10 Photograph of multi-point temperature recorders

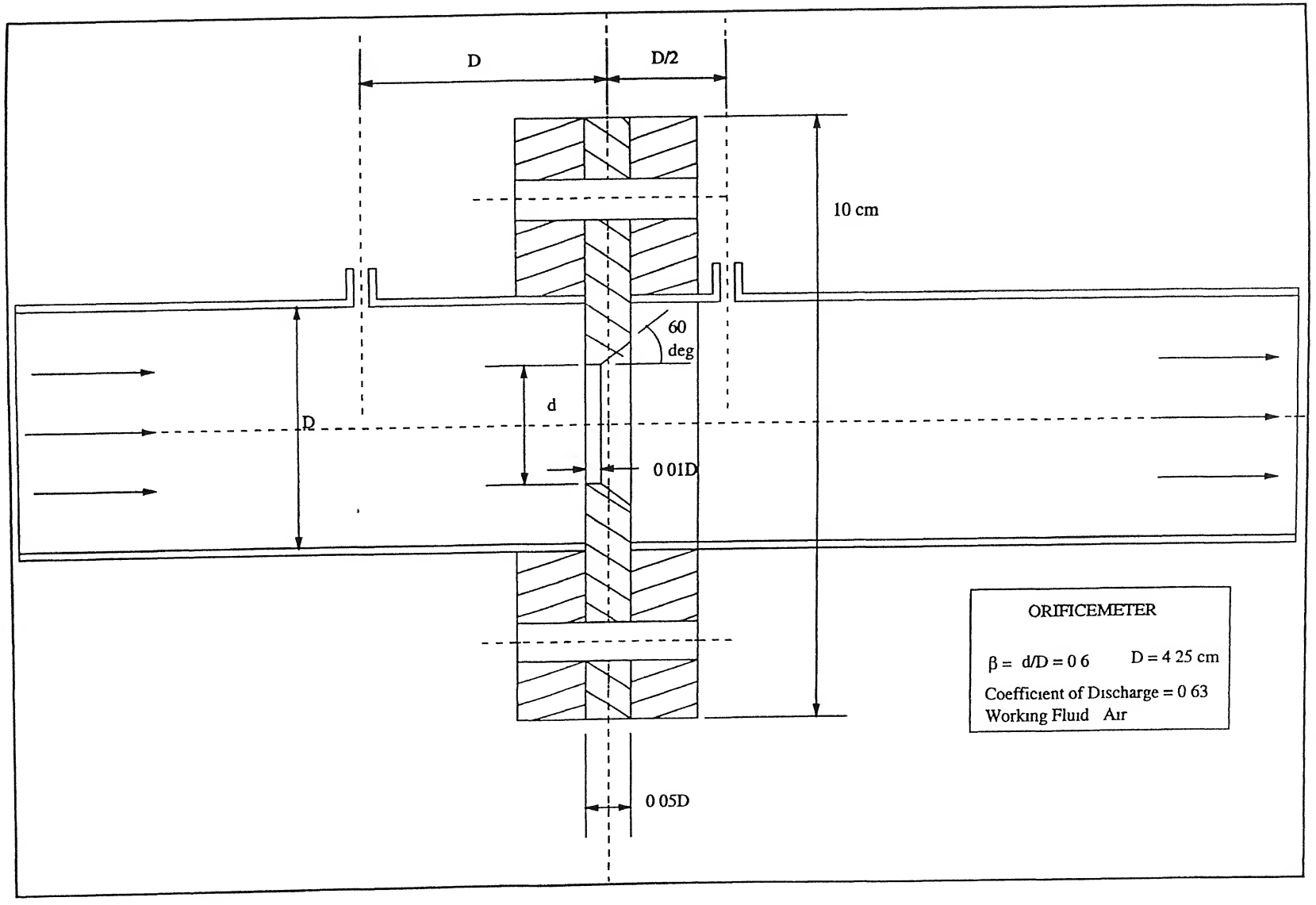

Fig. 3.11 Schematic view of orifice meter

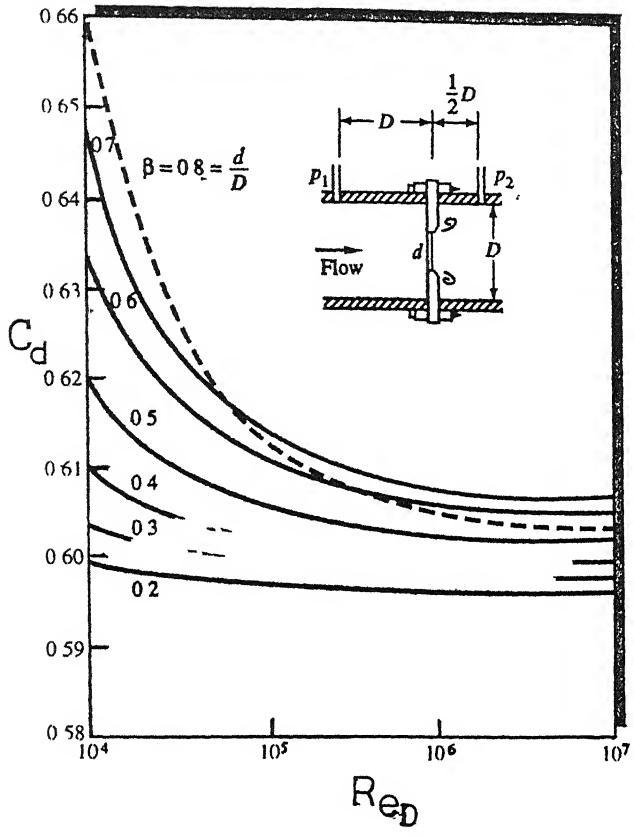

Fig 3 12 Discharge coefficient for a thin plate orifice with D $\frac{1}{2}D$ taps

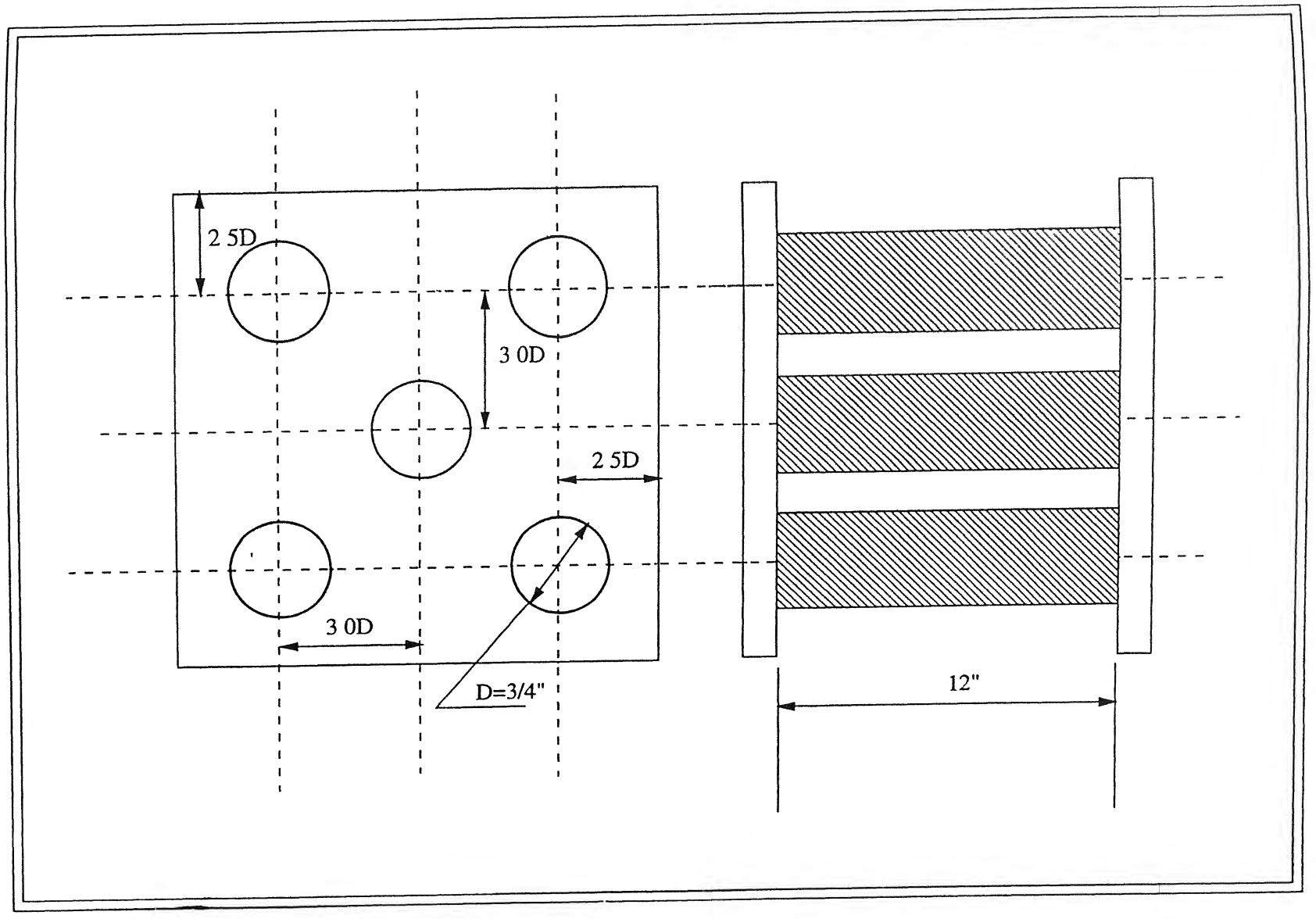

Fig. 3.13 Schematic view of orientation of the heating coils

CHAPTER 4

TEST PROCEDURE AND DATA REDUCTION

4.1 Introduction

As already stated, the objective of the study was to experimentally investigate jet-crossflow interaction which is representative of the film cooling applications So, it has been decided to measure velocity fields and adiabatic surface temperatures over a plate created due to relatively hot secondary air injection We have chosen two types of hole-configuration straight hole with 0° compound angle (CA), and skewed hole with CA=35° with the streamwise direction, both set of holes are inclined at 35° to the surface

4.2 Measurement of velocity profiles

Centerline velocity fields were measured with straight hole (CA = 0°) only Total pressure readings were taken at three *x/D* locations for the values of blowing ratio of 0 5 and 1 0 The RPM of the blower was set at 1100 for which the free stream velocity was calculated to be 17 9 *m/s* The probe movement was confined along the centerline in the *x-y* plane by the traverse mechanism To study the nature of the flow fields at upstream and downstream of injection, velocity profiles were measured at *x/D* = –3 5, 5 0, 10 0 and 15 0 Total pressure within the boundary layer was measured by a pitot tube of 0 3 *mm* tip diameter and pressure readings were obtained from an inclined tube manometer It has also been observed that the static pressure along the tunnel length was almost constant So, the static pressure measured at the mean location of the test section was used as the reference static pressure for boundary layer calculations The schematic view of boundary layer pressure measurement is shown in Fig 4 1

Now,

$$p_1 + \rho\frac{u^2}{2} = p_2 \tag{4 1}$$

$$\Rightarrow\ p_2 - p_1 = \rho\frac{u^2}{2} \tag{4 2}$$

$$\Rightarrow\ u = \sqrt{\frac{2(p_1 - p_2)}{\rho}} \tag{4 3}$$

where, p_1 = static pressure, and p_2 = total pressure This u represents local velocity within the boundary layer

From calculated velocity at various *y* positions, velocity plots were drawn for all the three *x/D* locations To evaluate the nature of approach boundary layer, the displacement thickness (δ^*), the momentum thickness (δ^{**}) and the shape factor (H) were calculated by numerical integration for $x/D = -3\,5$

$$\delta^* = \sum_{i=1}^{n-1}\left(1 - \frac{u_i}{U_\infty}\right)(y_{i+1} - y_i) \tag{4 4}$$

$$\delta^{**} = \sum_{i=1}^{n-1}\frac{u_i}{U_\infty}\left(1 - \frac{u_i}{U_\infty}\right)(y_{i+1} - y_i) \tag{4 5}$$

$$H = \frac{\delta^*}{\delta^{**}} \tag{4 6}$$

4.3 Measurement of surface temperature

Surface temperatures were measured for different blowing and temperature ratios and expressed non-dimensionally in terms of adiabatic film effectiveness (Eq 1 3) as,

$$\eta_{ad} = \left(\frac{T_{aw} - T_\infty}{T_j - T_\infty}\right)$$

where, T_{aw} is the adiabatic wall temperature sensed by PRTDs, located at 34 points downstream of injection. T_∞ is the free stream temperature measured at 15*D* upstream of the injection Centerline effectiveness and effectiveness for the line of symmetry between two holes were

plotted against x/D for various density and blowing ratios and compared with each other to study the effect of density ratio and blowing ratio on effectiveness

T_j is the temperature of injected jet at the hole exit, calculated from the measured temperature (T_p) of air inside the plenum chamber and jet velocity (V_j) Jet velocity was calculated from volume flow rate indicated by the orifice meter placed at secondary circuit The value of V_j is obtained as under

The flow rate, Q was obtained from orifice meter (Eq 3 6),

$$Q = 1\ 50332 \times 10^{-3} \sqrt{\frac{(\Delta h)}{\rho_j}}\ m^3/s \tag{4 7}$$

where, Δh is the pressure difference shown by the U-tube manometer in *mm of water* This flow rate must passes through the discrete injection holes and finally mixes with the cross flow Thus,

$$V_j = Q/A_j = \frac{1\ 50332 \times 10^{-3}}{A_j} \times \sqrt{\left(\frac{\Delta h}{\rho_j}\right)} \tag{4 8}$$

where, ρ_j = Density of jet at the exit of hole, A_j=Total projected area of injection

Here, heat loss between the exit of heater and the plenum chamber was neglected, and the air temperature at the exit of heater was assumed to be almost equal to that of the plenum chamber Furthermore, density variation of blowing air between stagnation and static conditions was neglected

Thus we can write, $$T_j = T_p - \frac{V_j^2}{2c_p} \tag{4 9}$$

where T_j, T_p and V_j are already defined and c_p is the specific heat of air at constant pressure

Blowing ratio was varied by changing the volume flow rate of hot air From Eq 1 1, we have

$$BR = \frac{\rho_J V_J}{\rho_\infty V_\infty} \quad \text{or} \quad BR = \left(\frac{\rho_J}{\rho_\infty V_\infty}\right) V_J \tag{4 10}$$

The study was performed for one fixed rpm of the main blower So, ρ_∞ and V_∞ were fixed Now, for a particular value of T_p, ρ_J is also fixed The only parameter by which the blowing ratio can be varied is the jet velocity From Eqs 4 8 and 4 10, we get

$$BR = \frac{1\,50332\times10^{-3}}{A_J} \times \left(\frac{\rho_J}{\rho_\infty V_\infty}\right) \times \sqrt{\frac{\Delta h}{\rho_J}} \tag{4 11}$$

The above equation can be written as,

$$BR = C_0 \sqrt{\Delta h} \tag{4 12}$$

where, $$C_0 = \frac{1\,50332\times10^{-3}}{A_J} \times \left(\frac{\sqrt{\rho_J}}{\rho_\infty V_\infty}\right) = \text{constant}$$

Thus, the blowing ratio can easily be calculated by using the Eq 4 12 It is also clear that we can vary the blowing rate by changing the volume flow rate of the secondary blowing circuit All the results are presented for the steady state conditions

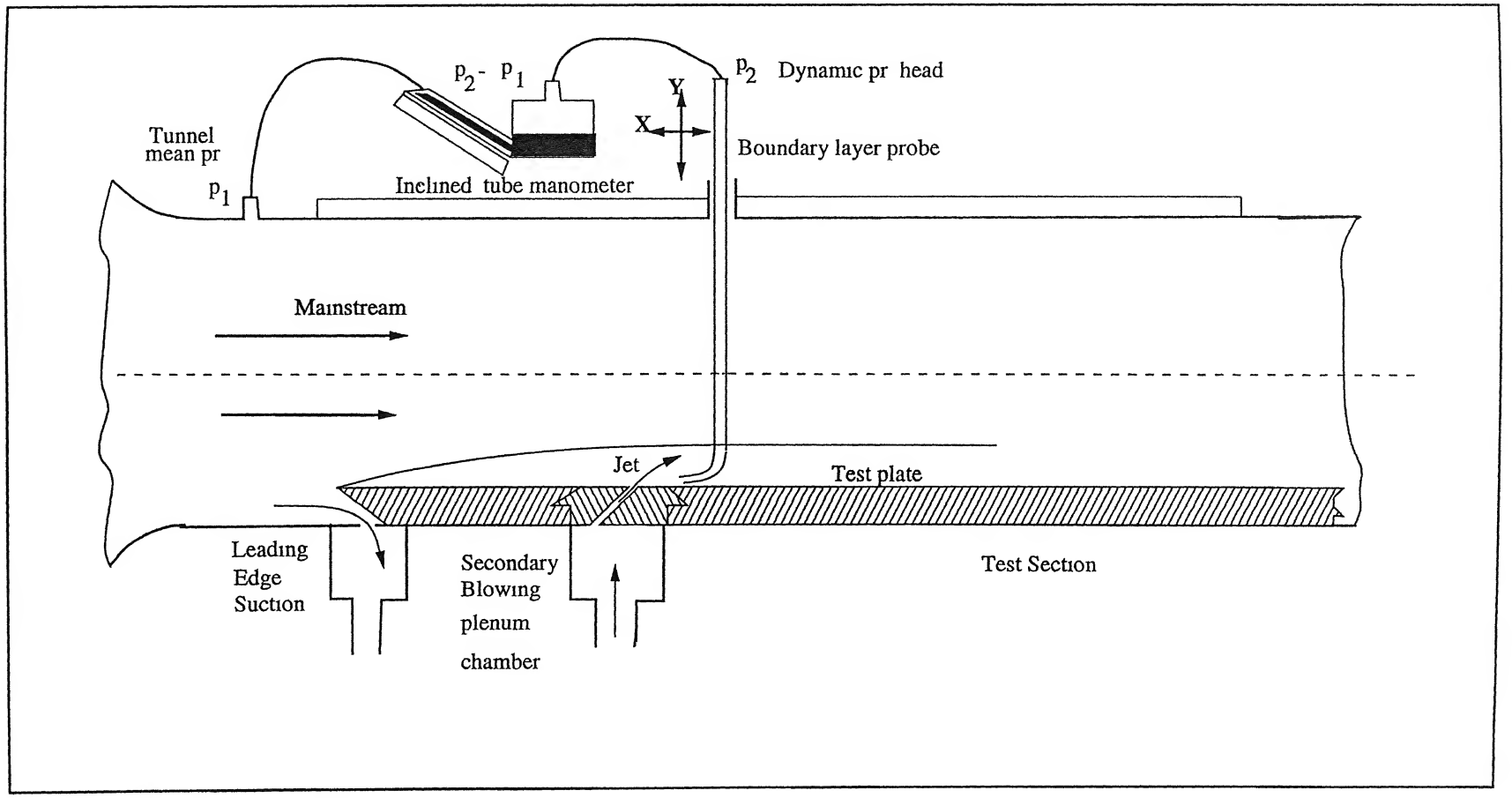

Fig. 4.1 Schematic view of boundary layer measurement

CHAPTER 5

PRESENTATION AND DISCUSSION OF RESULTS

5.1 Introduction

All the measurements were taken for a mainstream velocity of 17 9 *m/s* for which the Reynolds number based on hole diameter (D) was $R_{e_D} = 0\ 12\times10^5$ This Reynolds number, R_{e_D} when converted for a characteristic length, $\tilde{L} = 1\ m$, becomes, $R_{e_\infty} = R_{e_D} \times \left(\frac{\tilde{L}}{D}\right) = 1\ 2\times10^6$ For the analysis of jet cross flow interaction, the experiment was performed for the following parameters·

$$BR = 0\ 5,\ 1\ 0 \text{ and } 1\ 44,$$

$$T_p = 40°,\ 50°, \text{ and } 60°\,C$$

Two discrete hole-configurations were used one with 0^0 compound angle and another is a skewed hole with 60^0 compound angle with respect to the x-direction, as shown in Fig 5 1(a) and 5 1(b) Angle of injections, 35^0, remained same for both the hole-configurations

5.2 Velocity fields

Results were presented along x (streamwise) and z (crosswise) directions, where the origin was located at the center of the projected ellipse of the center hole on the flat surface The y-direction has been chosen normal to the flat surface

To represent the character of boundary layer at the upstream and the downstream of injection holes, velocity profiles were measured at different stations x/D = –3 5, 5.0, 10.0, and 15 0 for two different blowing ratios Velocity fields were measured only for holes with 0^0 C A Figure 5 2 shows the velocity profiles for blowing ratio of 0 5 The profiles at different locations are presented in Fig 5 2 (a), (b), (c), and (d) To investigate the

characteristics of the approach boundary layer, on which the effectiveness is dependent, the *shape factor* (H) was calculated after evaluating the *displacement thickness* (δ^*), and *momentum thickness* (δ^{**}) The calculated values of δ^*, δ^{**} and H are given below

$$\delta^* = 6\ 63\ mm\ ,\ \delta^{**} = 5\ 02\ mm\ ,\ H = 1\ 32\ (H < 2\ 5)$$

From the above value of H, it can be inferred that the approach boundary layer was turbulent as the estimated value of *shape factor* was close to 1 4 Figure 5 2 (b), (c), and (d) indicate the shape of velocity profiles downstream of injection The momentum deficit zone is very clear at x/D = 5 0, depicting a shear layer between the jet and the mainstream crossflow At far downstream (x/D = 10 0, and 15 0), velocity profiles gradually become boundary layer like profiles

The shear layer developed due to jet-crossflow interaction along the centerline downstream of the holes for higher blowing ratio of, BR = 1 0 is represented in Fig 5 3 Here, the momentum deficit zone is clearer, indicating enhanced jet penetration and increased near-field three-dimensionality due to high jet velocity Again at far stream (x/D = 15 0), the velocity profile resembles a boundary layer profile due to mixing of jets, Fig 5.3(d)

5.3 Film effectiveness

Adiabatic film effectiveness (η_{ad}, as described in Eq 1 3) as a function of dimensionless co-ordinate x/D are represented for different blowing and temperature ratios along the centerline of the center hole (z/D = 0) and also along the line of symmetry between two holes (z/D = 1 5) The variations of effectiveness as shown in this work were directly calculated from the measured surface temperature, ignoring the error that would occur due to conduction, however small it may be As already stated, the conductivity of the material used for the test plate was 0 01 - 0 02 $W/m\,K$, which is practically very small Thus, the plate has been assumed to be adiabatic.

5.3.1 Hole configuration with 0^0 C.A.

All the results presented in this section deal with the hole-configuration where the compound angle is 0^0 that is there is no skewness, however, angle of injection is 35^0

Figure 5 4 shows the variation of the adiabatic film effectiveness along the centerline (z/D = 0) and line of symmetry between the holes (z/D = 1 5) for $B\,R$ = 0 5 and $T_p = 40\,^\circ C$ which gives a density ratio of $D\,R$ = 0 936 The freestream condition was T_∞=15 5 ^{0}C and V_∞= 17 9 *m/s* The effectiveness between the two holes in the near-field region is shown to be much lower as compared to the values of the effectiveness along the centerline of holes This is due to sideways ventilation of the mainstream between two discrete jets Far downstream, the variations of both the effectiveness along the centerline and along the line of symmetry become identical, indicating the decrease in three-dimensionality

Figure 5 5 illustrates the variation of film effectiveness for the same conditions as in Fig 5 4, except the blowing ratio, which has been increased from 0 5 to 1 0 in this case This figure also indicates that the variation of effectiveness along the line of symmetry between two holes is much less than that along the centerline of holes, illustrating the strong lateral variation of effectiveness in the near-field region Thus in the near-field, there exist a temperature gradient in the z direction which is not desirable Another important point is to be noted that very near to the injection, where x/D<5 0, effectiveness along the centerline starts drooping This may be connected to the fact that at high blowing ratio, the injected jet tends to detach from the surface due to high jet penetration, resulting into a local separation bubble just ahead of the blowing hole Flow reattaches the surface at about x/D = 5 0 in this case, indicating enhanced effectiveness The near-field average effectiveness also decreases for this condition i e , $B\,R$ = 1 0, compare to previous result where $B\,R$ = 0 5, due to high jet penetration which promotes more mixing However, the far-field effectiveness has enhanced due to more available injectant compared to the low blowing ratio

To illustrate the effect of blowing ratio on jet penetration, the variation of effectiveness along the centerline and along the line of symmetry between two holes have been superimposed in Fig 5 6(a) and 5 6(b) respectively, for BR = 0 5, 1 0, and 1 44 The density ratio is kept constant As blowing ratio is increased, the near-field effectiveness along the centerline as well as the line of symmetry decreases indicating *jet-lift-off* (detachment of jet from the surface) mechanism However, at far-stream the effectiveness increases because of more mixing and more available hot air, as blowing ratio is increased from 0 5 to 1 0 Further increase of blowing ratio also decreases downstream effectiveness due to pronounced mixing caused by very high jet penetration Thus, for the present hole-configuration, the average effectiveness is better for BR = 1 0 compare to other two cases

Fig 5 7 (a) and (b) describe the effects of blowing ratios as illustrated in the previous figure but for the lower density ratio (D R = 0 908) Here also jet penetration increases indicating low near-field effectiveness with increase in blowing ratio

Figure 5 8 (a) and 5 8 (b) shows the effect of density ratio on the variation of film effectiveness along the centerline and the line of symmetry between holes for B R = 1 0 Density ratio was varied by changing the temperature of blowing The overall effectiveness is comparatively higher both along z/D = 0 and z/D = 1 5 at high density ratio i e for injection with relatively colder air However, the jet penetration remains almost same since blowing ratio was unaltered, which is reflected by similar trend in the variation of effectiveness for different density ratios

The effect of density ratio on the variation of film effectiveness is shown by Fig 5 9 (a) and 5 9 (b) for high blowing ratio (B R = 1 44) As compared to the previous result it illustrate that the effect of density ratio is not felt in the variation of effectiveness except very near-to the injection This may possibly due to high mixing and jet penetration for higher blowing rate Thus, pronounced mixing between two jets suppresses the beneficial effect of density ratio

5.3.2 Hole configuration with 60° C.A.

The surface temperatures were measured for skewed holes with 60^0 compound angle In this case, the angle of injection was 35^0 as in the previous one All other geometric and flow parameters remained unchanged for the skewed hole It can be presumed that the skewed hole due to its configuration generates a lateral component of jet velocity along with its streamwise component This would enhance the lateral diffusion of jets and it has been thought that the near-field non-uniformity in the lateral variation of effectiveness could be reduced

Figures 5 10, 5 11, 5 12, and 5 13 represent the film effectiveness downstream of a row of skewed holes at various density and blowing ratios These figures depict that the variation of film effectiveness along the centerline of a hole and that along the symmetry line between two holes are almost identical This illustrate that the near-field non-uniformity in lateral variation of effectiveness due to sideways mainstream ventilation, as observed in the case of non-skewed holes, has been successfully removed However, in the case of compound angle injection, mixing of flow was more which finally led to low average far-field effectiveness as compared to the corresponding studies with non-skewed holes

To compare the effect of blowing ratio on effectiveness, the variation of effectiveness along the centerline for skewed holes are superimposed in Fig 5 14 for blowing ratio, $B\,R$ = 0 5 and 1.0, and with a constant density ratio, $D\,R$ = 0 907 This confirms that for the configuration, $B\,R$ = 1 0 gives better effectiveness especially in the far-field area

The effect of density ratio on the variation of the effectiveness along the centerline of holes is shown in Fig 5 15 for $D\,R$ = 0 908 and 0 880, with a constant blowing ratio, $B\,R$ = 1 0 The overall effectiveness is much improved for higher density ratios, i e injection with relatively colder air

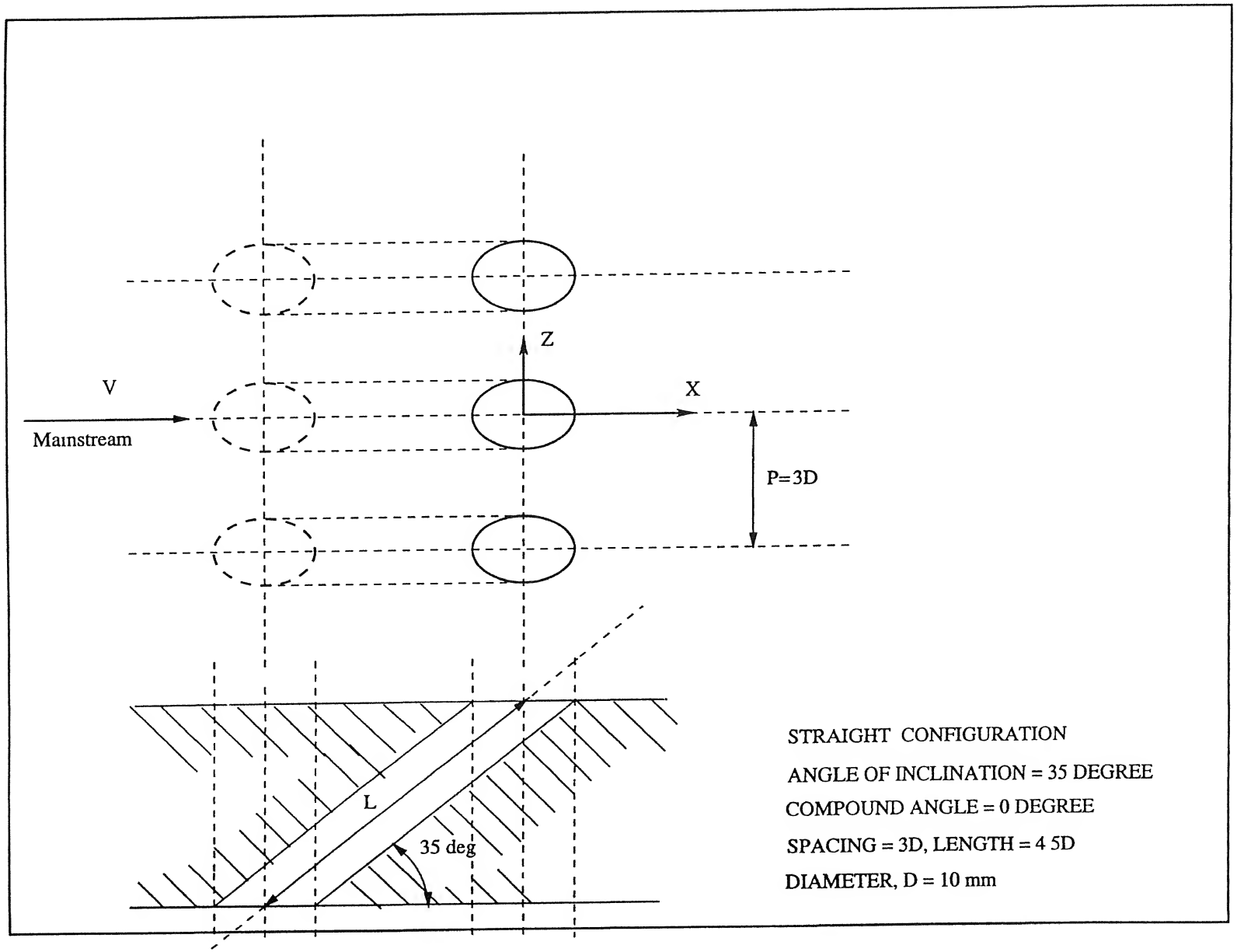

Figure 5.1(a) The schematic view of non skewed hole configuration

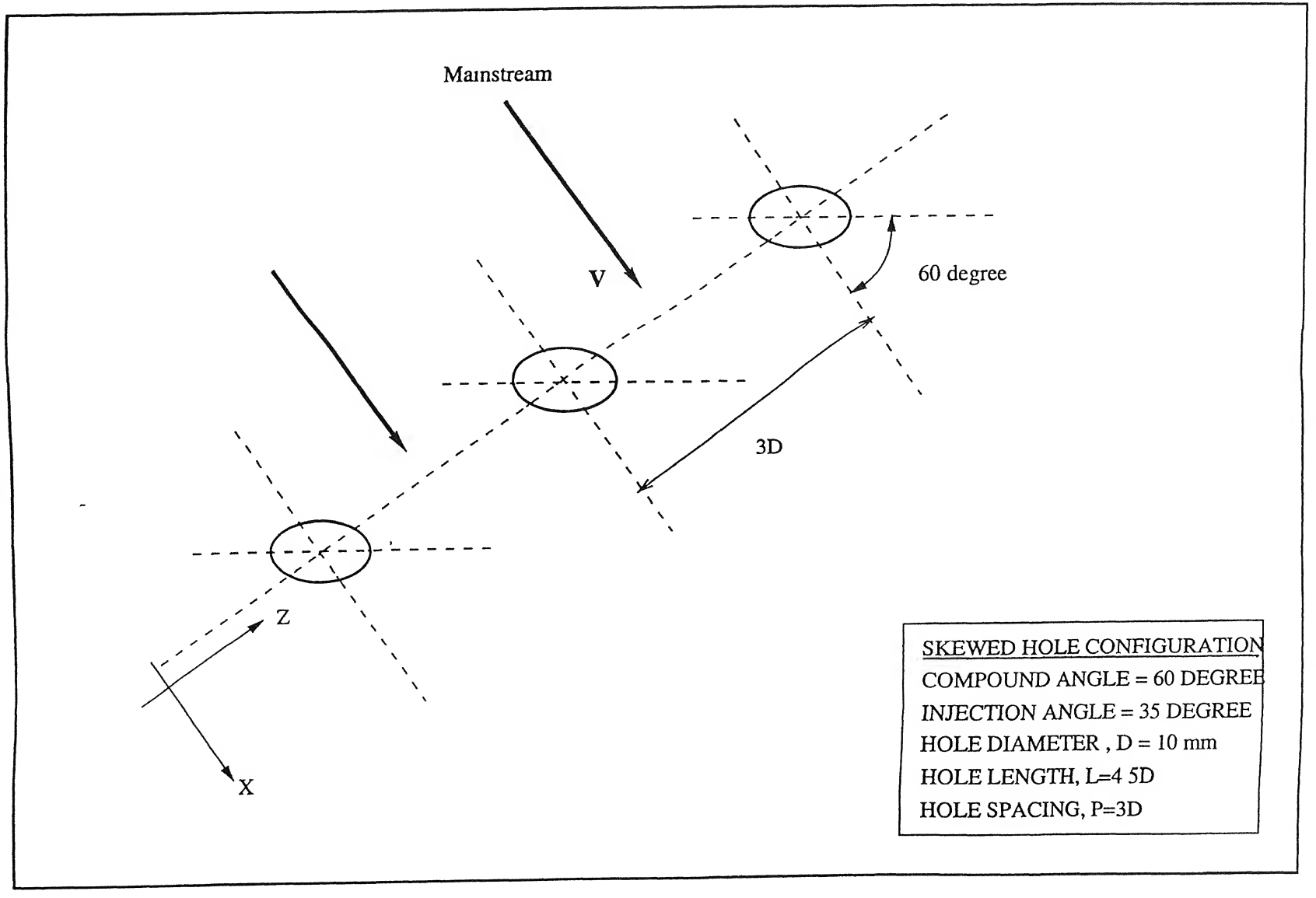

Fig. 5.1(b) Schematic view of skewed hole configuration

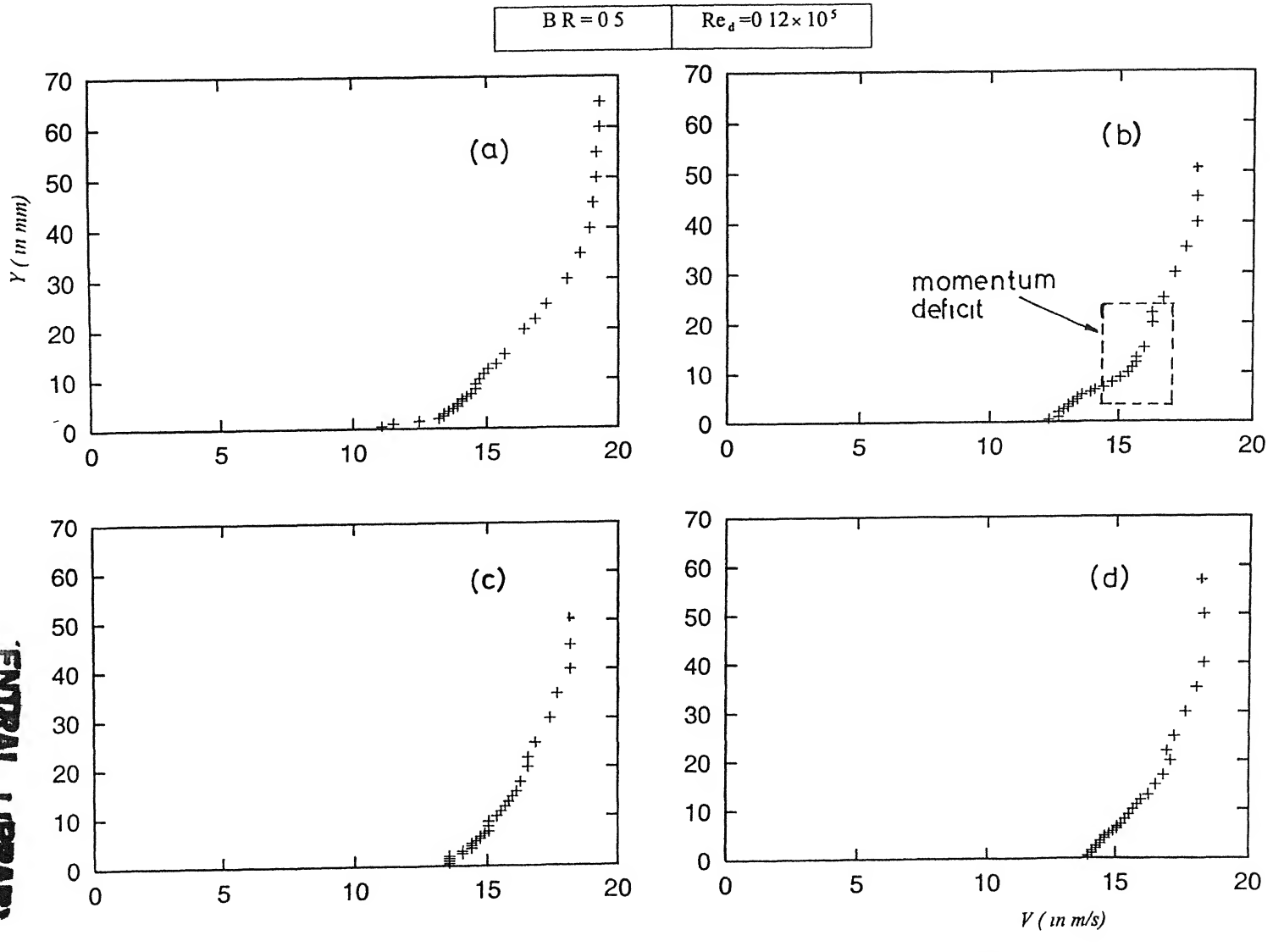

Fig 5 2 Centerline velocity profile downstream of a row of holes with 0^0 C A

(a) at x/D=-3 5 (without blowing); (b), (c), and (d) at x/D = 5, 10, and 15, for B R =0 5

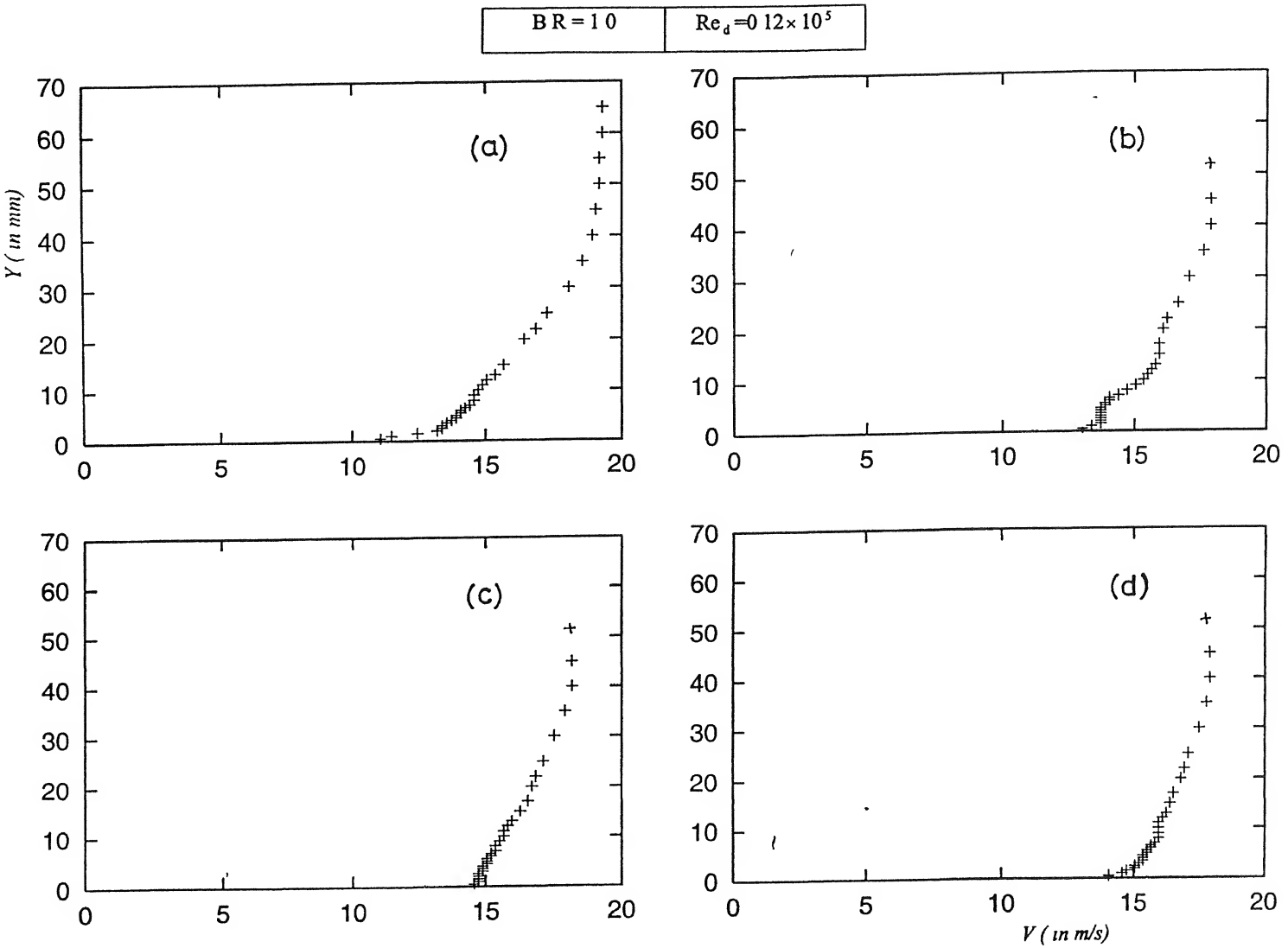

Fig 5 3 Centerline velocity profile downstream of a row of holes with 0^0 C A (a) at x/D=-3 5 (without blowing), (b), (c), and (d) at x/D = 5, 10, and 15, for B R =10

$T_p = 40^0 C$	$DR = \frac{\rho_J}{\rho_\infty} = 0936$	$BR = \frac{\rho_J V_J}{\rho_\infty V_\infty} = 05$

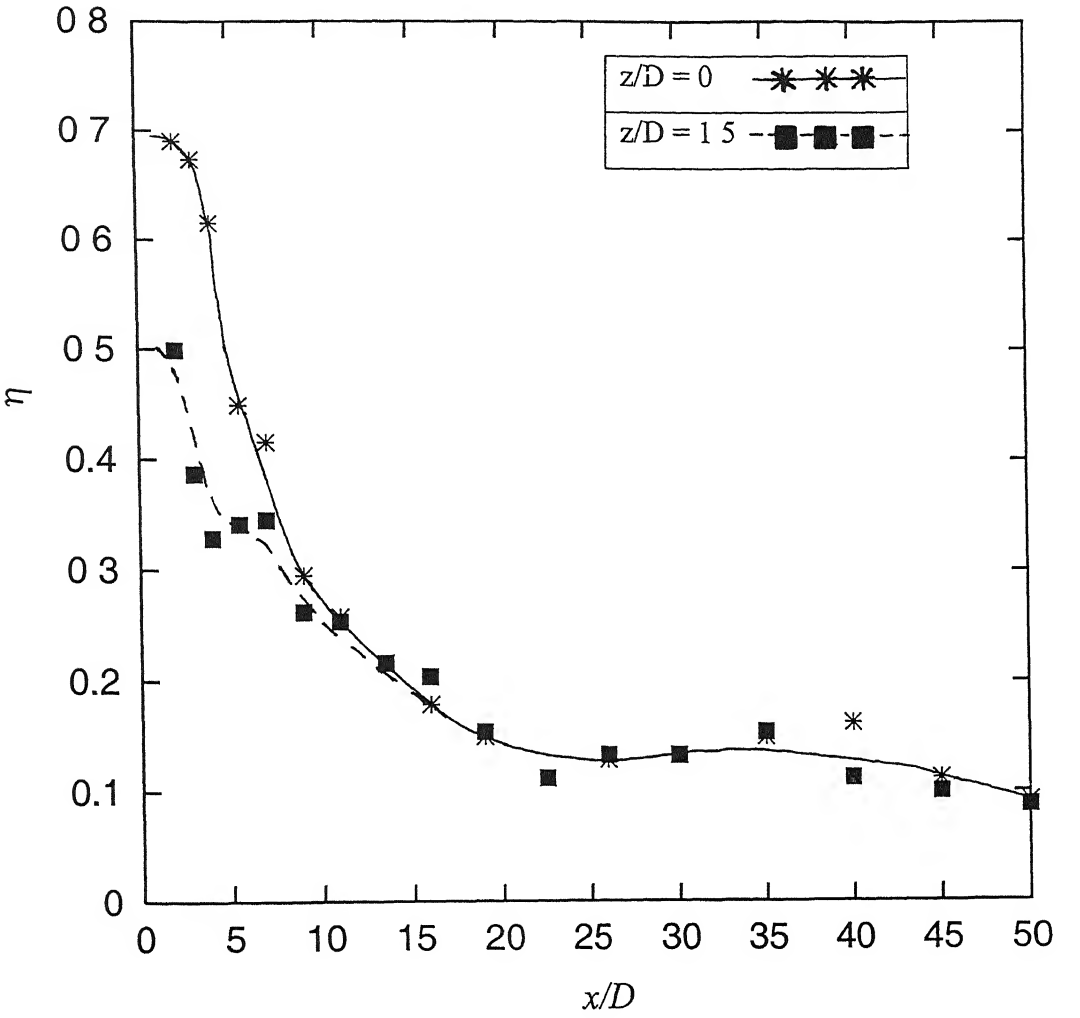

Fig 5 4 Film effectiveness downstream of a row of holes for B R =0 5

$T_p = 40^0 C$	$DR = \frac{\rho_J}{\rho_\infty} = 0.937$	$BR = \frac{\rho_J V_J}{\rho_\infty V_\infty} = 1.0$

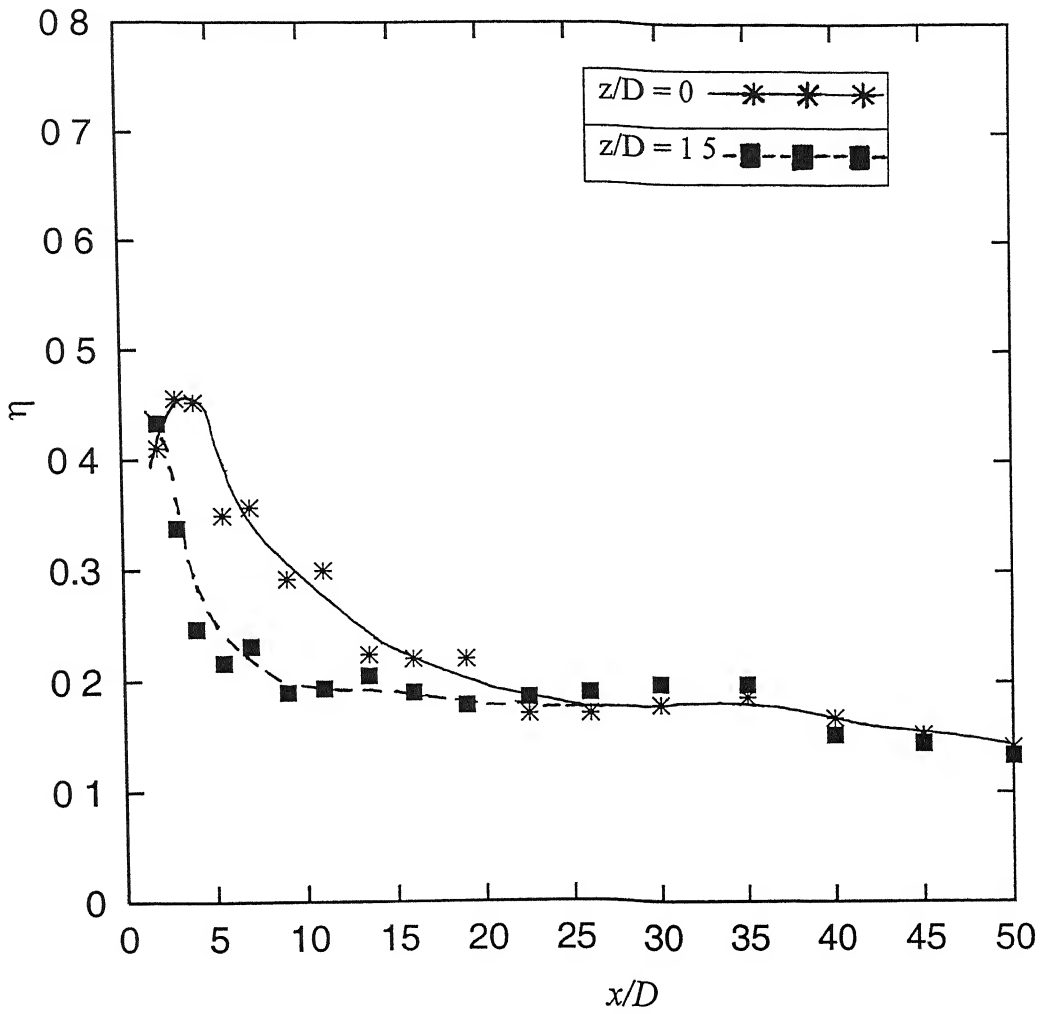

Fig 5.5 Film effectiveness downstream of a row of holes for B R =1.0

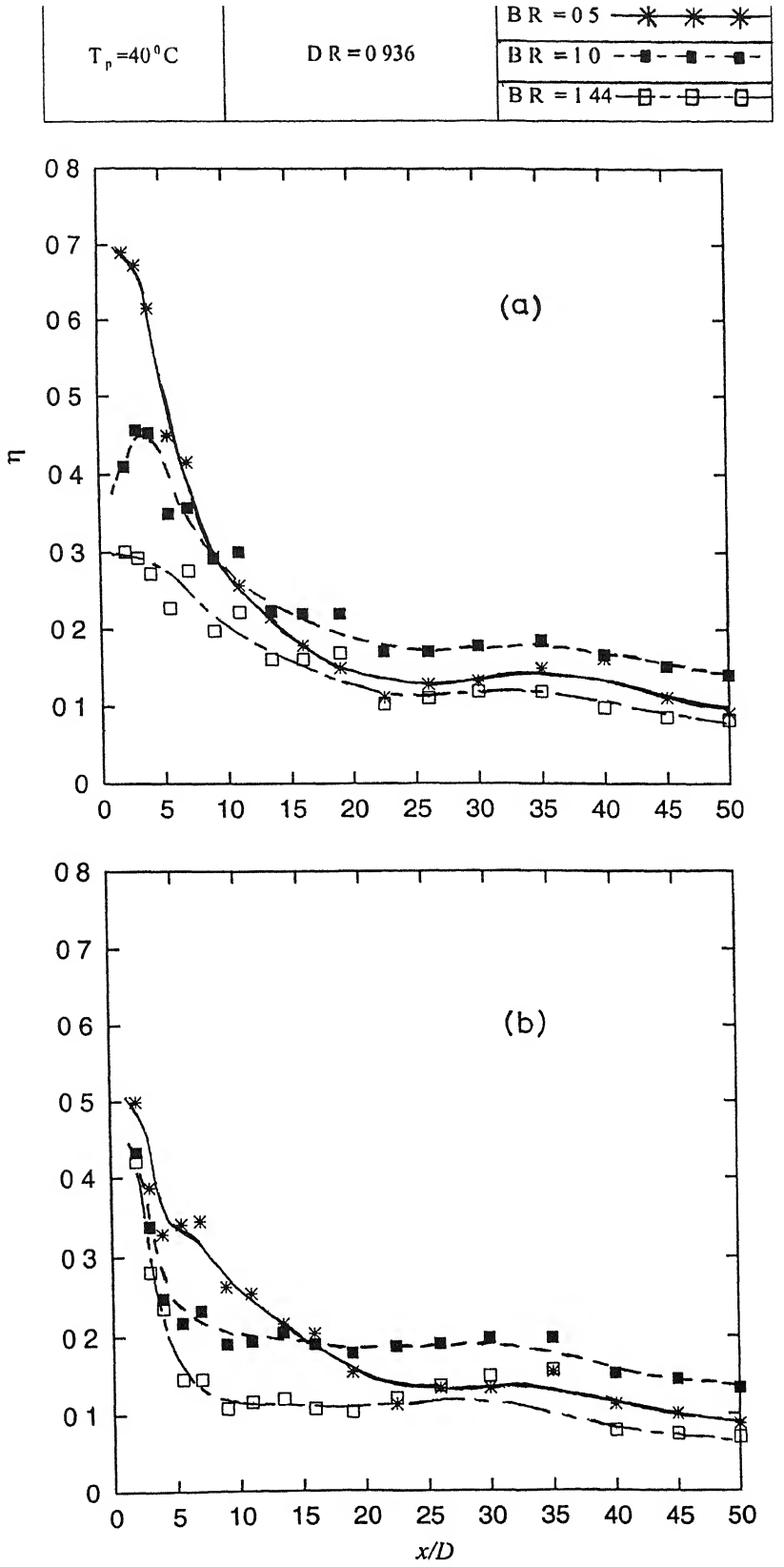

Fig 5 6 Streamwise variation of effectiveness (D R = 0 936) Effect of blowing ratio,

(a)along the centerline (z/D = 0),

(b)along the line of symmetry between two holes (z/D = 1 5)

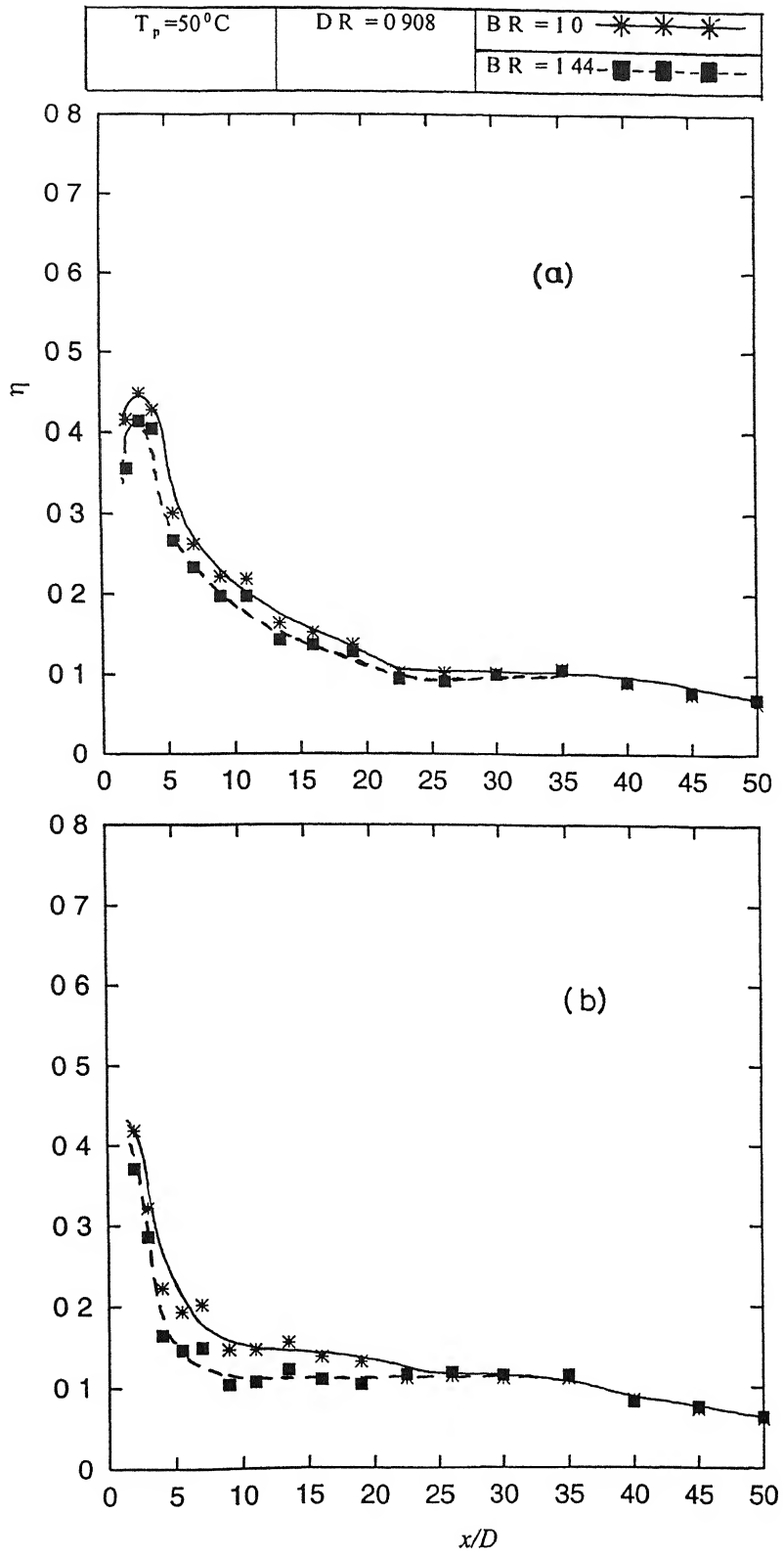

Fig 5 7 Streamwise variation of effectiveness (D R = 0 908) Effect of blowing ratio,

(a) along the centerline (z/D = 0),

(b) along the line of symmetry between two holes (z/D = 1 5)

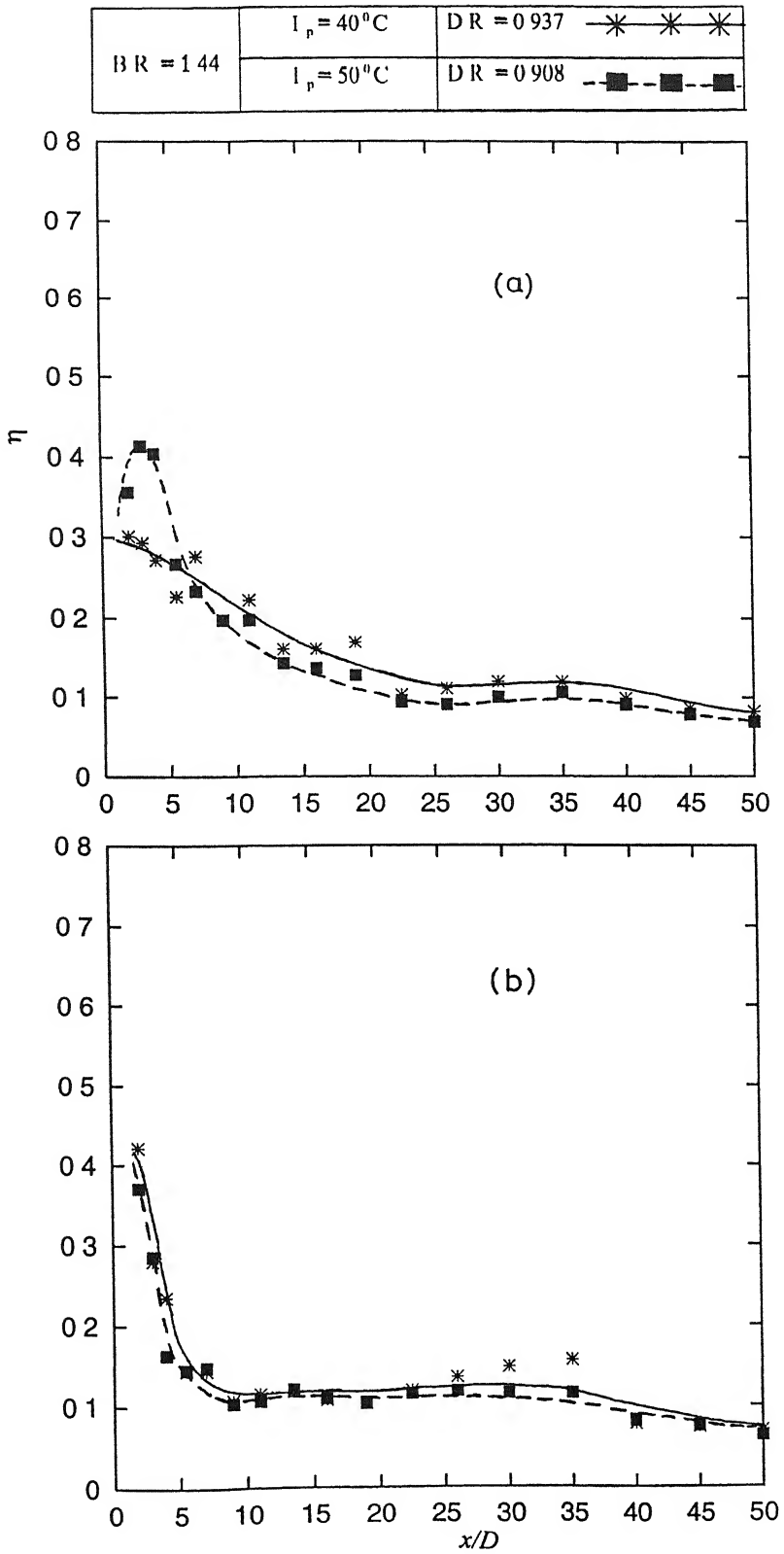

Fig 5 9 Streamwise variation of effectiveness (B R = 1 44) Effect of density ratio,

(a)along the centerline ($z/D = 0$),

(b) along the line of symmetry between two holes (z/D=1 5)

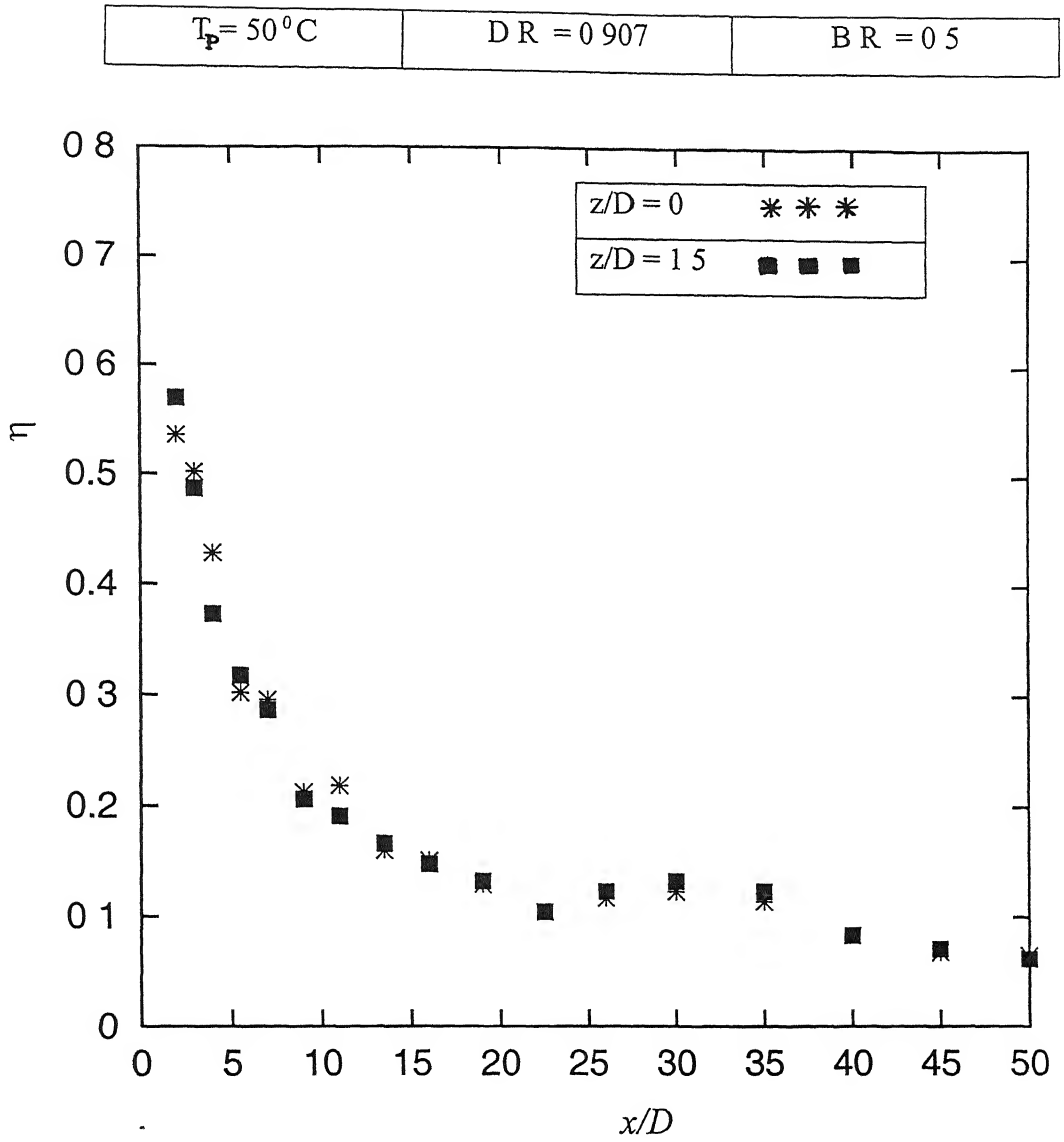

Fig 5 10 Film effectiveness downstream of a row of skewed holes for B R = 0 5, and D R = 0 907

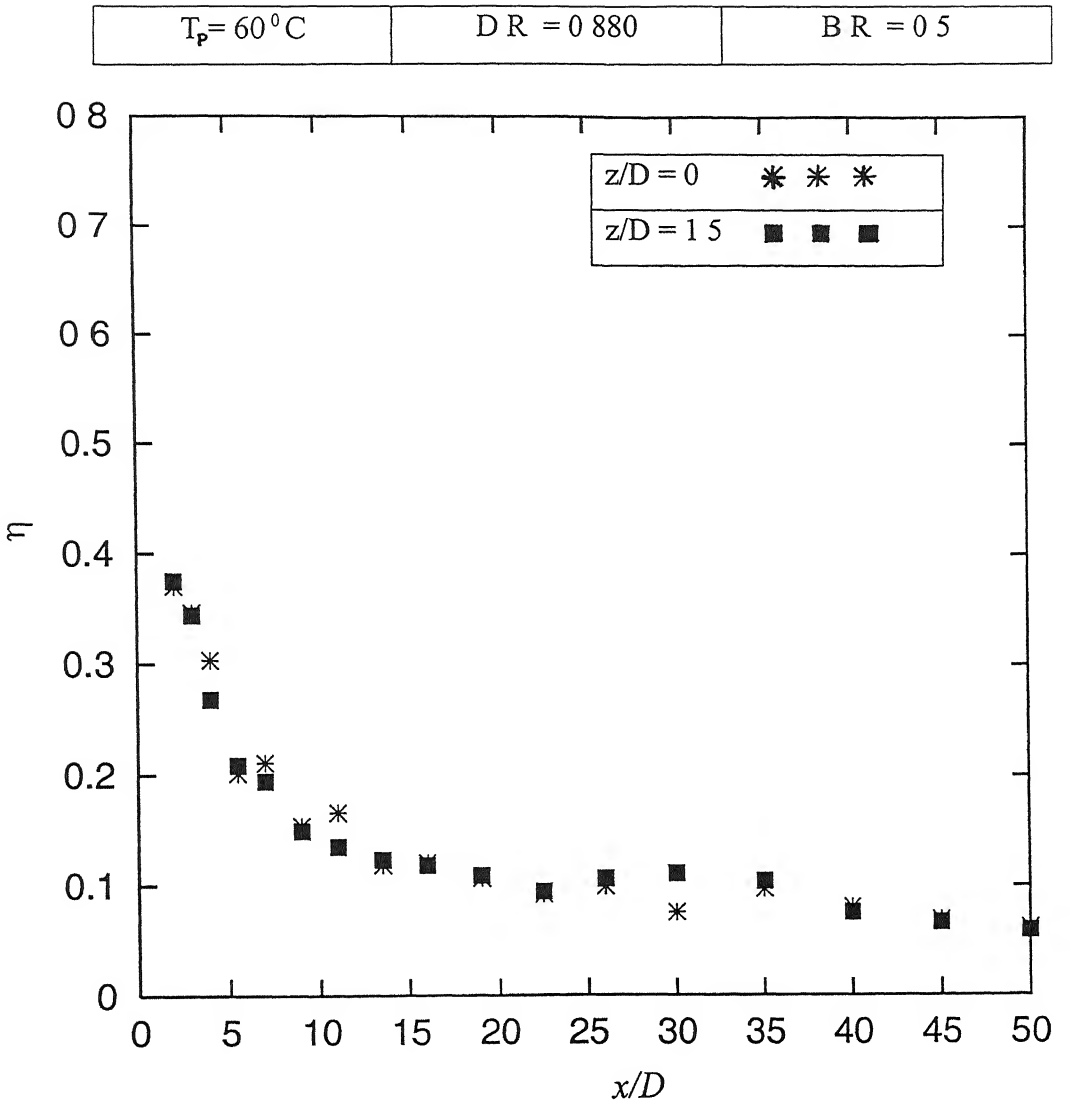

Fig 5 11 Film effectiveness downstream of a row of skewed holes for B R = 0 5, and D R = 0 880

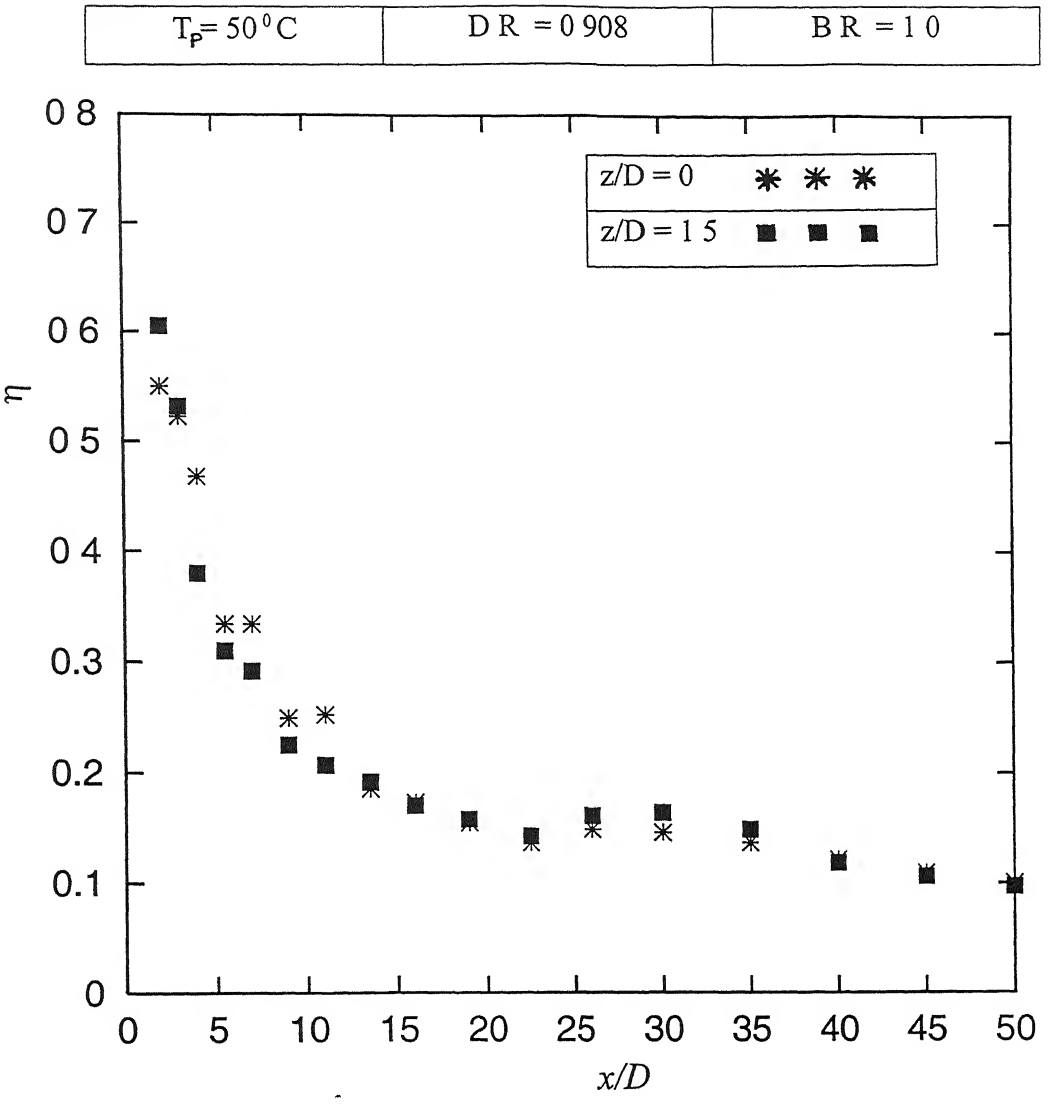

Fig 5 12 Film effectiveness downstream of a row of skewed holes for B R = 1 0, and D R = 0 908

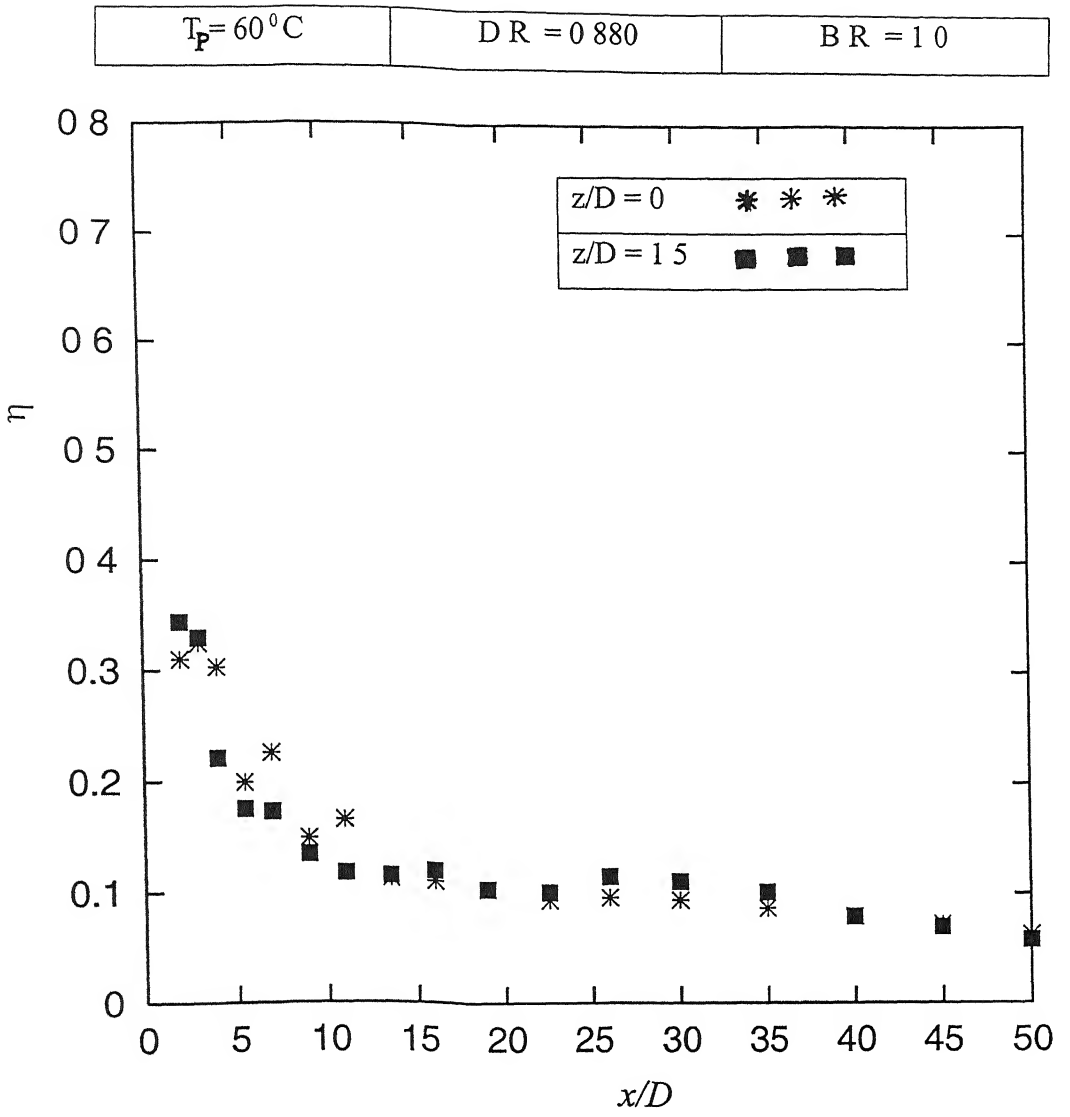

Fig 5 13 Film effectiveness downstream of a row of skewed holes for B R = 1 0, and D R = 0 880

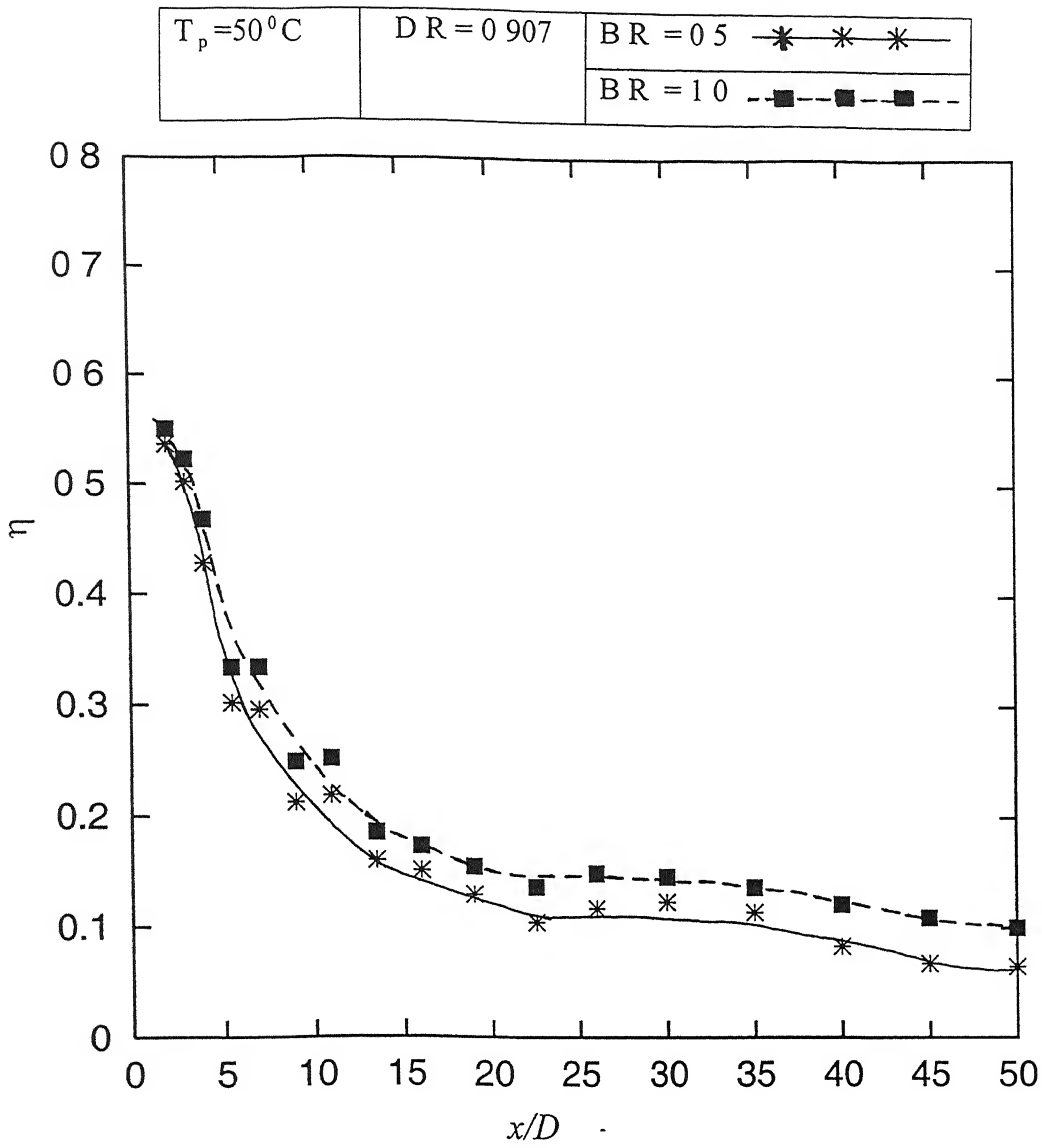

Fig 5 14 Streamwise variation of effectiveness along the centerline, downstream of a row of skewed holes (D R =0 907) Effect of blowing ratio

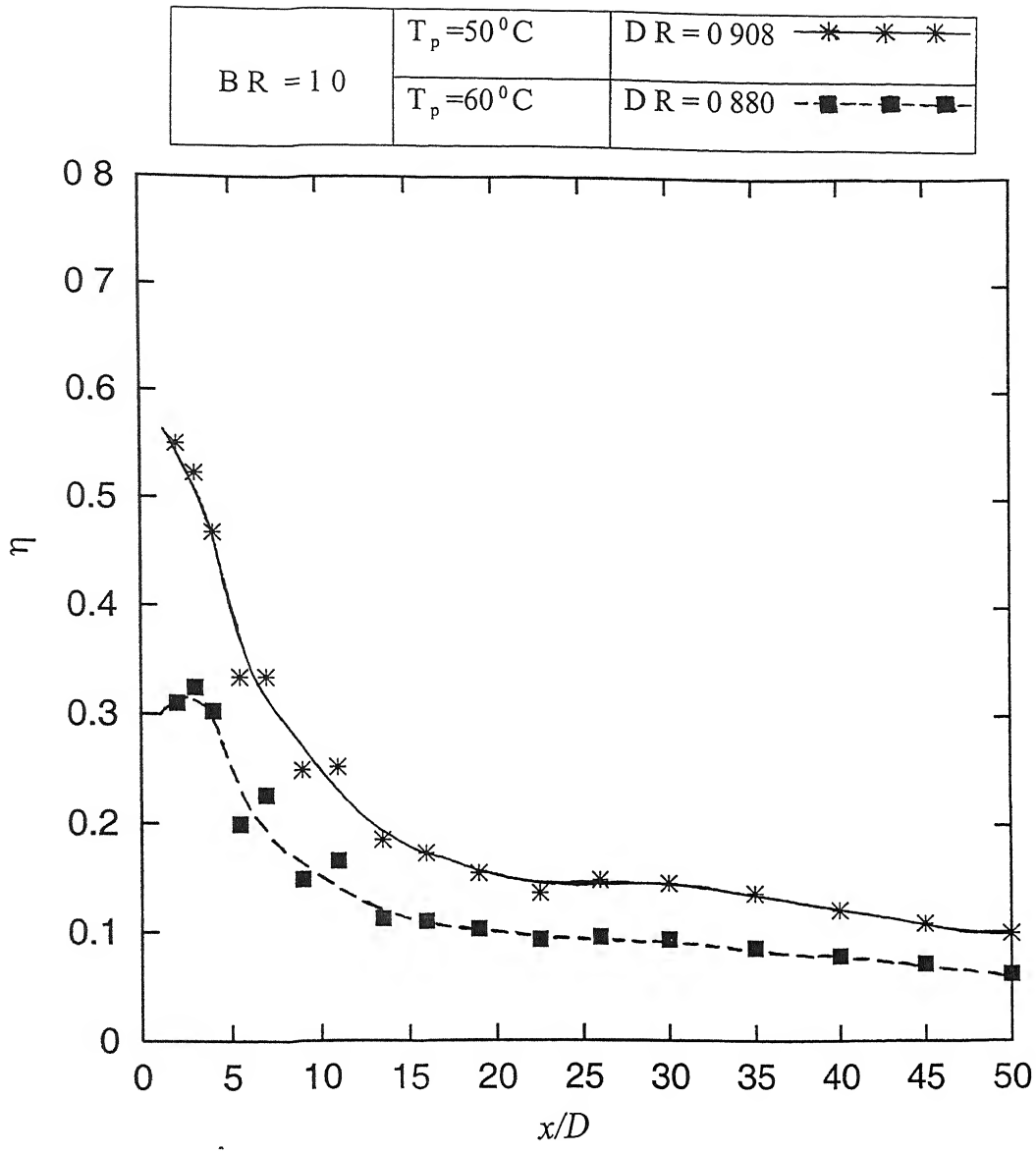

Fig 5 15 Streamwise variation of effectiveness along the centerline, downstream of a row of skewed holes (B R =1 0) Effect of density ratio

CONCLUSION

6.1 Conclusion

The aim of the present work was to experimentally investigate the aerodynamic and heat transfer aspects of jet-crossflow interactions over a flat plate with different hole configurations One of the major engineering applications of jet in crossflow is film cooling of gas turbine blades and walls However, it has been decided to inject hot secondary jets into a cold mainstream and thus to create a temperature gradient between the two streams The velocity profiles and surface temperatures were measured over a flat plate with a row of skewed and non-skewed holes for different blowing and density ratios

Results were presented in terms of velocity profiles and adiabatic film effectiveness From the velocity profiles it can be concluded that there exists a momentum deficit zone which occurs due to the formation of shear layer between the injected jet and the mainstream The near-field region also shows strong three-dimensionality But as the downstream is approached, the velocity profiles gradually tends to be boundary layer type profiles indicating a thorough mixing of two layers

To illustrate the performance of jet-crossflow interactions, the surface temperatures are represented in terms of film effectiveness along the centerline of holes and line of symmetry between two holes The results clearly depict the influence of blowing and density ratios on the effectiveness, both for skewed and non-skewed holes For a row of non-skewed holes with angle of injection 35^0, a strong variation in lateral effectiveness has been observed due to sideways ventilation As blowing ratio is increased from 0 5 to 1 0, the overall effectiveness improves, however, further increase in blowing ratio deteriorates the overall performance due to strong jet penetration and pronounced mixing Increase in density ratio is always beneficial With skewed

effectiveness suffers a bit due to enhanced mixing In this case also, the overall effectiveness is better for blowing ratio, $BR = 1.0$, and increase in density ratio is also beneficial Although, the skewed holes overcome the undesirable non-uniformity in the variation of effectiveness, one should assess the increase in aerodynamic loss related to compound angle

6.2 Suggestions for future work

Truly speaking, this is a first hand work to investigate the performance of jet-crossflow interaction on a set up which has been fabricated as a part of the thesis work Due to lack of time, it was not possible to perform a thorough experimentation A lot of work can be done and extended in different aspects of jet-crossflow interactions pertaining to film cooling with a little modification of the existing tunnel A brief list of the future directions is given below

(a) To investigate the influence of freestream turbulence on the performance of jet-crossflow interaction
(b) To study the dynamics of jet in crossflow with sophisticated instrumentation like LDV and hot-wire anemometer
(c) An error analysis should be carried out while calculating the effectiveness due conduction of heat between two consecutive temperature sensors fixed on the test plate

CALIBRATION OF *PRTD*100

CHART 5.1

(*PRTD* 100 s tested on the first day)

Water bath temperature measured by glass-thermometer (in °C)	Temperature(in °C) sensed by the *PRTD* 100 and recorded in digital temperature recorder Different *PRTD*s are designated as *1, 2, 3,*												
	1	*2*	*3*	*4*	*5*	*6*	*7*	*8*	*11*	*12*	*13*	*14*	*15*
31	31	31 5	31·5	31 7	31 6	31 6	31 4	31 5	31 4	31 6	31 7	31 5	31 4
40	39 8	40 7	40 7	40 7	40 8	40 9	40 8	40 8	40 4	40 6	40 9	40 7	40 6
60	60 5	60 2	60 1	59 8	60 0	59 9	60 5	60 4	60 5	60 3	60 4	60 2	60 3
80	81 0	81 0	79 8	80 6	81 0	80 4	81 0	81 0	80 6	80 8	80 4	79 9	81 0

CHART 5.2

(*PRTD*100 s tested on the second day)

Water bath temperature measured by glass-thermometer (in °C)	Temperature(in °C) sensed by the *PRTD* 100 and recorded in digital temperature recorder Different *PRTD*s are designated as *16, 17, 18,*									
	16	*17*	*18*	*19*	*20*	*21*	*22*	*23*	*24*	*25*
42	41 8	42 0	41 8	42 0	42 1	42 1	42 1	41 7	42 1	42 2
60	61 0	60 4	60 7	60 7	61 0	61 0	61 0	60 9	60 7	60 6
80	80 3	79 8	80 6	79 7	80 1	80 2	81 0	80 9	81 0	80 5

CHART 5.3

(*PRTD*100 s tested on the third day)

Water bath temperature measured by glass-thermometer (in ^{0}C)	Temperature(in ^{0}C) sensed by the *PRTD* 100 and recorded in digital temperature recorder. Different *PRTDs* are designated as *26, 27, 28,*									
	26	*27*	*28*	*29*	*30*	*31*	*32*	*33*	*34*	*35*
41	41 5	41 6	41 6	41 6	41 6	41 6	41 7	41 7	41 7	41 8
62	62 2	62 3	62 2	62 2	62 2	62 2	62 3	62 4	62 3	62 3
81	81 5	81 7	81 7	81 6	81 7	81 6	81 7	81 8	81 7	81 8

CHART 5.4

(*PRTD*100 s tested on the third day)

Water bath temperature measured by glass-thermometer (in ^{0}C)	Water bath temperature measured by electronic-thermometer (in ^{0}C)	Temperature(in ^{0}C) sensed by the *PRTD* 100 and Recorded in digital temperature recorder. Different *PRTDs* are designated as 9, *10, 36*		
		9	*10*	*36*
40 5	40 7	41 2	41 3	41 0
61 0	61 5	61 5	61 6	61 2
80 0	80 6	81 0	80 8	80 9

REFERENCES

1 Goldstein, R J , Eckert, E R G , and Burgraffand, F , (1972), Effects of Hole Geometry and Density on Three Dimensional Film Cooling, *Int Journal of Heat Mass Transfer*, Vol 17, pp 595-607

2 Pedersen, D R ,Eckert, E R G ,and Goldstein, R J , (1977), Film Cooling With Large Density Difference Between the Mainstream and the Secondary Fluid Measured by the Heat-Mass Transfer Analogy, *Tansaction of the ASME, Journal of Turbomachinery* Vol 99, pp 620-627

3 Foster, N W , and Lampard, D , (1980), The Flow and Flim Cooling Effectiveness Following Injection through a Row of Holes, *Transaction of the ASME, Journal of Turbomachinery*, Vol 102, pp ,584-588

4 Hay, N., Lampard, D , and Saluja, C L , (1985), Effects of the Condition of the Approach Boundary Layer and of Mainstream Pressure Gradients on the Heat Transfer Coefficient on Film-Cooled Surfaces, *Journal of Engineering for Gas Turbines and Power* Vol 107, pp 99-104

5 Hay, N , Lampard, D , and Saluja, C L , (1985), Effects of Cooling Film on The Heat Transfer Coefficient on a Flat Plate With Zero Mainstream Pressure Gradient, *Journal of Engineering for Gas Turbines and Power* Vol 107, pp 105-110

6 Goldstein, R J ,Eckert, E. R G , Chiang, H D ,and Elovic, E , (1985), Effects of Surface Roughness on Film Cooling Performance, *Journal of Engineering for Gas Turbines and Power* Vol 107, pp 111-116

7 Jurban, B , and Brown A , (1985), Film Cooling From Two Rows of Holes Inclined in the Streamwise and Spanwise Directions, *Transaction of the ASME, Journal of Turbomachinery* Vol 107, pp 84-91

8 Schiffer, H P , and Hennecke, D K , (1991), The Influence of Gas Temperature on Turbine Blade Film Cooling Effectiveness Determined with Model Testing, *Third European Propulsion Forum*

9. Sinha, A K , Bogard, D G , and Crawford, M E , (1991), Film-Cooling Effectiveness Downstream of a Single Row of Holes With Variable Density Ratio, *Transaction of the ASME, Journal of Turbomachinery* Vol 113, pp 442-449

10 Pena, L F , and Arts, T , (1992), On The Development of A Film Cooling Layer, von Karman Institute for Fluid Dynamics

11 Ligrani, P M , Ciriello, S , and Bishop, D T , (1992), Heat Transfer, Adiabatic Effectiveness, and Injectant Distributions Downstream of a Single Row and Two Staggered Rows of Compound Angle Film-Cooling Holes, *Transactions of the ASME, Journal of Turbomachinery* Vol 114, pp 687-700

12 Honami, S , Shizawa, T , and Uchiyama, A , (1994), Behaviour of the Laterally Injected Jet in Film Cooling Measurements of Surface Temperature and Velocity/Temperature field Within the Jet, *Transactions of ASME, Journal of Turbomachinery* Vol 116, pp 106-112

13 Jabbari, A L , Marston, K C , Eckert, E R G , and Goldstein, R J , (1996), Film Cooling of the Gas Turbine endwall by Discrete-Hole Injection, *Transactions of the ASME, Journal of Turbomachinery* Vol 118, pp 278-284

14 Sen, B , Schmidt, D L , and Bogard, D G , (1996) , Film Cooling With Compound Angle Holes Heat Transfer, *Transactions of the ASME, Journal of Turbomachinery* Vol 118, pp 800-806

15 Sen, B , Schmidt, D L , and Bogard, D G , (1996) , Film Cooling With Compound Angle Holes Adiabatic Effectiveness, *Transactions of the ASME, Journal of Turbomachinery* Vol 118, pp 807-813

16 Wang, H P , Olson, S J ,Goldstein, R J , and Eckert, E R G , (1997), Flow Visualization in a Linear turbine Cascade of High Performance Turbine Cascade, *Transactions of the ASME, Journal of Turbomachinery* Vol 119, pp 1-8

17. Kohli, A , and Bogard, D G, (1997) , Adiabatic Effectiveness, Thermal Fields, and Velocity Fields for Film Cooling With Large Angle Injection, *Transactions of the ASME, Journal of Turbomachinery* Vol 119, pp 352-358

18 Goldstein, R J , and Stone, L D , (1997), Row-of-Holes Film Cooling of Curved Walls at Low Injection Angles, *Transactions of the ASME, Journal of Turbomachinery* Vol 119, pp 574-579

19 Ligrani, P M , and Ramsey, A E , (1997) , Film Cooling From Spanwise Oriented Holes in Two Staggered Rows, *Transactions of the ASME, Journal of Turbomachinery* Vol 119, pp 562-567

20 Ligrani, P M , Gong, R , and Cuthrell, J M , (1997) ,Bulk Flow Pulsations and Film Cooling Flow Structure Just Downstream of the Holes, *Transactions of the ASME, Journal of Turbomachinery* Vol 119, pp 568-573

21 Ligrani, P M , and Ramsey, A E , (1997) , Film Cooling From a Single Row of Holes Oriented in Spanwise/ Normal Planes, *Transactions of the ASME, Journal of Turbomachinery* Vol 119, pp 770-776

22 Friedrichs, S , Hodson, H P , and Dawes, W N , (1997) , Aerodynamics Aspects of Endwall Film Cooling, *Transactions of the ASME, Journal of Turbomachinery* Vol 119, pp 786-793

23 Giel, P W , Thrman, D R , Van Fossen, G J , Hippensteele, S A , and Boyle, R J , (1998) , Endwall Heat Transfer Measurements in a Transonic Turbine Cascade, *Transactions of the ASME, Journal of Turbomachinery* Vol 120, pp 305-313

24 Goldstein, R J , Olson, R L ,and Jin, P , (1999), Film Cooling Effectiveness and Mass/ Heat Transfer Coefficient Downsteram of One Row of Discrete Holes, *Transactions of the ASME, Journal of Turbomachinery* Vol 121, pp 225-232

25 Bird, S W , and Simon, T W , (1999), Measurements of Discharge Coefficient in Film Cooling, *Transactions of the ASME, Journal of Turbomachinery* Vol 121, pp 243-248

26 Seo, H J , Lee, J S , and Ligrani, P M , (1999) , Effects of Bulk Flow Pulsations on Film Cooling From Different Length Injection Holes at Different Blowing Ratios, *Transactions of the ASME, Journal of Turbomachinery* Vol 121, pp 542-550

27 Goldstein, R J , (1971), "Film Cooling", *Advances in Heat Transfer*, Academic Press, New York and London, pp 321-379

28 White, F M , (1994) , Fluid Mechanics, 3rd Edition, *McGraw-Hill Inc*